EISCAT

EUROPEAN INCOHERENT SCATTER
SCIENTIFIC ASSOCIATION

ANNUAL REPORT 2023–2024

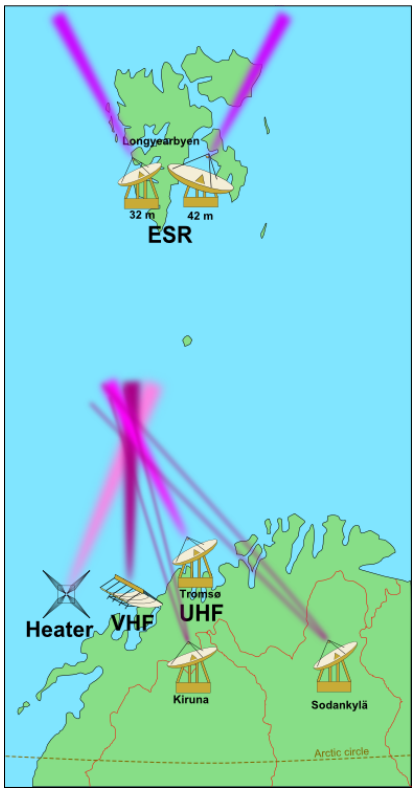

EISCAT Radar Systems

Location		Tromsø	Kiruna	Sodankylä	Longyearbyen	
Geographic coordinates		69°35′N 19°14′E	67°52′N 20°26′E	67°22′N 26°38′E	78°9′N 16°1′E	
Geomagnetic inclination		77°30′N	76°48′N	76°43′N	82°6′N	
Invariant latitude		66°12′N	64°27′N	63°34′N	75°18′N	
Band	UHF	VHF	VHF	VHF	UHF	
Frequency (MHz)	929	224	224	224	500	
Maximum bandwidth (MHz)	8	3	8	8	10	
Transmitter	2 klystrons	1 klystron	-	-	16 klystrons	
Channels	6	6	6	6	12	
Peak Power (MW)	2.0	1.6	-	-	1.0	
Average power (MW)	0.25	0.20	-	-	0.25	
Pulse duration (ms)	0.001–2.0	0.001–2.0	-	-	0.0005–2.0	
Phase coding	binary	binary	binary	binary	binary	
Minimum interpulse (ms)	1.0	1.0	-	-	0.1	
Digital processing	14 bit ADC on IF, 32 bit complex autocorrelation functions, parallel channels					
					Antenna 1	**Antenna 2**
Antenna	parabolic dish 32 m steerable	parabolic cylinder 120 m × 40 m steerable	parabolic dish 32 m steerable	parabolic dish 32 m steerable	parabolic dish 32 m steerable	parabolic dish 42 m fixed
Feed system	Cassegrain	line feed 128 crossed dipoles	crossed dipole	crossed dipole	Cassegrain	Cassegrain
System temperature (K)	90	250	100	100	80	65
Gain (dBi)	48.1	46	35.4	35.4	42.5	44.8
Polarisation	circular	circular	any	any	circular	circular

EISCAT Heating Facility (Tromsø)

Frequency range: 4.0 MHz to 8.0 MHz, Maximum transmitter power: 12×0.1 W, Antennas: Array 1 (5.5 MHz to 8.0 MHz) 30 dBi, Array 2 (4.0 MHz to 5.5 MHz) 24 dBi, Array 3 (5.5 MHz to 8.0 MHz) 24 dBi.
Additionally, a Dynasonde is operated at the heating facility.

Cover picture: Demolishing of the Kiruna receiver antenna, October 2024 (Photo: Martin Eriksson).

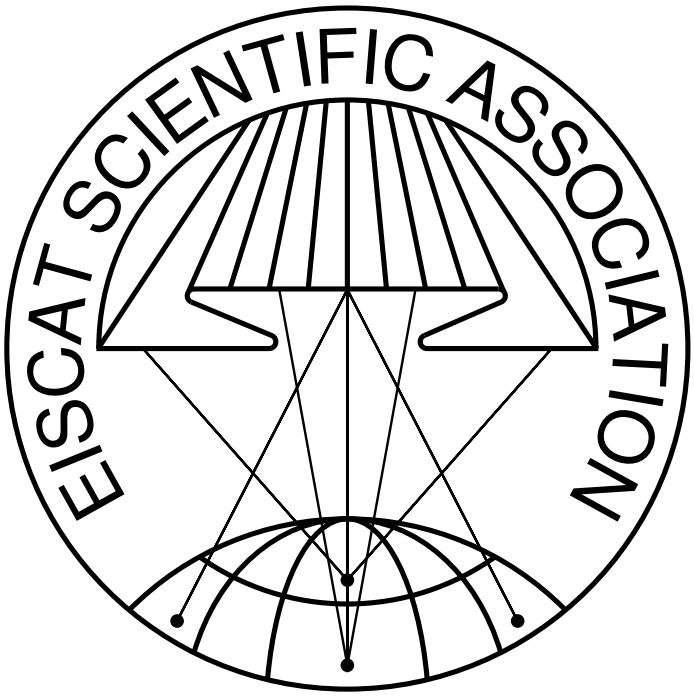

EISCAT Scientific Association
2023–2024

The EISCAT Scientific Association exists to provide scientists with access to incoherent scatter radar facilities of the highest technical standard

- *by developing and operating a continuing program of observatory measurements in cooperation with other ground-based and space-borne instruments and as part of the global network of incoherent scatter radars, the EISCAT Scientific Association seeks to provide a long-term database of ionospheric measurements of the highest quality.*
- *by supporting and operating the particular experiments of individual, and groups of, visiting scientists, EISCAT seeks to allow its users to address the widest possible range of research activities particularly in the areas of geospace and basic plasma physics.*
- *by providing leadership in the design and construction of hardware and software to support these goals, the EISCAT Scientific Association seeks to provide educational opportunities for young scientists and to foster appropriate Knowledge Transfer and Economic Impact.*
- *by developing and maintaining a well-founded science strategy, EISCAT seeks to provide a framework for the development of EISCAT-supported science and for the evaluation and development of scientific programs within the overall field.*

The scientific strategy of EISCAT is to understand the various forms of coupling between the Sun, the interplanetary medium, the terrestrial magnetosphere, ionosphere, and atmosphere of the high-latitude regions, natural and anthropogenic forcing, and related plasma physics and dynamics, and to achieve the necessary knowledge, understanding, principles, and techniques which would allow mankind to monitor, predict, and mitigate such processes within the next 30 years.

The specific goals of EISCAT are to develop large-scale facilities, techniques, and methods and, together with other ground-based and space-borne instruments, and as part of the global network of incoherent scatter and other middle and upper atmosphere radars, to encourage and undertake high quality research related to the global goal through studies addressing

- *behaviour and energy budget of the high-latitude regions, including space weather effects.*
- *fundamental plasma physics and dynamic processes in the near-Earth space environment.*
- *trends in atmospheric and ionospheric conditions, including long-term global change.*
- *properties and dynamics of the interplanetary environment.*
- *parametrisation of these processes and the development of techniques for their prediction.*

The investments and operational costs of EISCAT are shared between:

China Research Institute of Radiowave Propagation, People's Republic of China
National Institute of Polar Research, Japan
Norges forskningsråd, Norway
Suomen Akatemia, Finland
UK Research and Innovation, United Kingdom
Vetenskapsrådet, Sweden

Contents

Scientific highlights and list of publications 2023–2024 **7**

Space and atmospheric physics on Svalbard: a case for continued incoherent scatter radar measurements under the cusp and in the polar cap boundary region 7

Effect of polar cap patches on the high-latitude upper thermospheric winds 7

Ionospheric upwelling and the level of associated noise at solar minimum 8

On the creation, depletion, and end of life of polar cap patches 8

Statistical comparison of electron precipitation during auroral breakups occurring either near the open-closed field line boundary or in the central part of the auroral oval . 9

Influence of meteoric smoke particles on the incoherent scatter measured with EISCAT VHF 10

Inferring neutral winds in the ionospheric transition region from atmospheric-gravity-wave travelling-ionospheric-disturbance (AGW-TID) observations with the EISCAT VHF radar and the Nordic Meteor Radar Cluster 11

On the factors controlling the relationship between type of pulsating aurora and energy of pulsating auroral electrons: Simultaneous observations by Arase satellite, ground-based all-sky imagers and EISCAT radar 11

Do the throat auroras create polar cap patches? 12

On mechanisms for high-frequency pump-enhanced optical emissions at 557.7 nm and 630.0 nm from atomic oxygen in the high-latitude F-region ionosphere 12

Atmospheric ionizations by solar X-Rays, solar protons, and radiation belt electrons in September 2017 space weather event 13

Volumetric Reconstruction of Ionospheric Electric Currents From Tri-Static Incoherent Scatter Radar Measurements 14

The first simultaneous spectroscopic and monochromatic imaging observations of short-wavelength infrared aurora of N_2^+ Meinel (0,0) band at 1.1 µm with incoherent scatter radar 14

Ionospheric fireworks illuminate auroral science 15

Application of generalised-aurora computed tomography to the EISCAT_3D project . . . 16

The high latitude ionospheric response to the major May 2024 geomagnetic storm: a synoptic view 16

The nature of electron density enhancement over a wide altitude range during ionosphere heating experiments at EISCAT 17

EISCAT Operations 2023–2024 **25**

EISCAT Organisational Diagram, 2024 **31**

Committee Membership and Senior Staff **33**

Appendix: EISCAT Scientific Association Annual Report, 2023 **35**

Appendix: EISCAT Scientific Association Annual Report, 2024 **47**

The EISCAT Associates and Affiliates, December 2024 **59**

Contact Information **60**

Scientific highlights and list of publications 2023–2024

Space and atmospheric physics on Svalbard: a case for continued incoherent scatter radar measurements under the cusp and in the polar cap boundary region

Baddeley et al. (2023) presented work forwarding a case for continued incoherent scatter radar measurements on Svalbard. The EISCAT Svalbard incoherent scatter radar (ESR), located just outside Longyearbyen (78.15°N) on Svalbard, is the only currently operating facility capable of making such measurements inside the polar cusp — an area of significant energy input into the atmosphere and characterized by heating instabilities and turbulence. The ESR was built in the mid-1990s and has provided valuable data for the international experimental and modelling communities. New radar technologies are now available, in the form of phased array systems, which offer new data products and operational flexibility. The paper outlines the achievements and current research focus of the ESR and provides scientific arguments (see Figure 1), compiled from inputs across the international scientific community, for a new phased array ISR facility on Svalbard. In addition to the fundamental scientific arguments, the paper discusses additional benefits of continued ISR observations on Svalbard, building on the key findings of the ESR. Svalbard has a large network of complementary instrumentation both focused on the MLTI system (eg the Kjell Henriksen auroral Observatory, the Svalbard SuperDARN radar and the Svalrak sounding rocket launch facility) with synergies to other research fields, such as meteorology and oceanography. As a further holistic system science view of the Earth becomes more important, a new ISR on Svalbard will be important also in this respect with its ability to provide datasets with a wide range of scientific applications. Increased activity in space has highlighted problematic issues such as space debris.

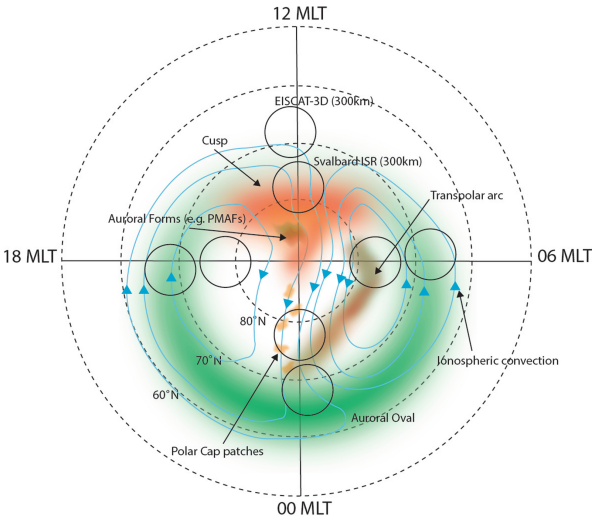

Figure 1: Magnetic Local Time (MLT) plot showing the location of both the Svalbard ISR and new EISCAT_3D fields of view (at 300 km) at 4 different MLT periods in relation to the main auroral oval and dayside cusp region. Other phenomena (such as polar cap patches) are also marked on for context.

A changing Arctic has also seen increased human activity via the opening up of new shipping routes, which are reliant on GNSS technology that is effected by severe turbulence in the MLTI system. As such, societal applications of a future ISR are also presented. The accessibility and logistical support for such a facility is also briefly discussed.

Effect of polar cap patches on the high-latitude upper thermospheric winds

A study by Cai et al. (2024) focuses on the poorly known effect of polar cap patches (PCPs) on the ion-neutral coupling in the F-region. The PCPs were identified by total electron content measurements from the Global Navigation Satellite System (GNSS) and the ionospheric parameters from the

Defense Meteorological Satellite Program spacecraft. The EISCAT incoherent scatter radars on Svalbard and at Tromsø, Norway observed that PCPs entered the nightside auroral oval from the polar cap and became plasma blobs (see Figure 2]). The ionospheric convection further transported the plasma blobs to the duskside. Simultaneously, long-lasting strong upper thermospheric winds were detected in the duskside auroral oval by a Fabry-Perot Interferometer (FPI) at Tromsø and in the polar cap by the Gravity Recovery and Climate Experiment satellite. Using EISCAT ion velocities and plasma parameters as well as FPI winds, the ion drag acting on neutrals and the time constant for the ion drag could be estimated. Due to the arrival of PCPs/blobs and the accompanied increase in the F-region electron densities, the ion drag is enhanced from about 220 km to 500 km altitudes. At the F peak altitudes near 300 km, the median ion drag acceleration affecting neutrals more than doubled and the associated median e-folding time decreased from 4.4 h to 2 h. The strong neutral wind was found to be driven primarily by the ion drag force due to large-scale ionospheric convection. The results provide a new insight into ionosphere-thermosphere coupling in the presence of PCPs/blobs.

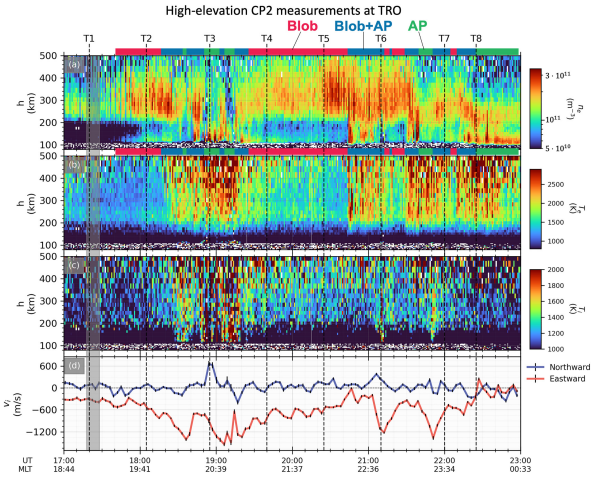

Figure 2: Ionospheric parameters measured by the Tromsø UHF radar, scanning with three high-elevation beams. Panels from top to bottom are the altitude profiles of (a) n_e, (b) T_e, (c) ion temperature T_i, (d) the northward (blue), and eastward (red) components of the ion velocity (v_i) in the F-region. The horizontal colour bars on the top panel indicate the times with the identifications of plasma blobs ("Blob" in red), auroral precipitation ("AP" in green), and a combination of Blob and AP (blue). The black shading indicates a quiet period and the n_e values within that are used as a background.

Ionospheric upwelling and the level of associated noise at solar minimum

David et al. (2024) have studied the ionospheric upwelling with a magnitude of above 10^{13} m^{-2} s^{-1} using the data during the European Incoherent Scatter Scientific Association (EISCAT) Svalbard Radar International Polar Year (IPY-ESR) 2007 campaign, which coincides with the solar minimum. The noise level in low-, medium- and high-flux upflows was investigated (see Figure 3). They found that the noise level in high-flux upflow is about 93 %, while in the low and medium categories it was 62 % and 80 % respectively. This showed that robust and stringent filtering techniques must be ensured when analysing incoherent data in order not to introduce bias to the result. Analysis reveals that the frequency of the low-flux upflow events was about 873 times the medium- and high-flux upflow events, respectively. Seasonal observation showed that the noise level in the upflow classes was predominantly high during winter. The noise was minimal in summer, with a notable result indicating occurrence of actual data above noise in the low-flux class. Moreover, the percentage occurrence of the noise level in the data increased with increasing flux strength, irrespective of the season. Further analysis revealed that the noise level in the local time variation peaked around 17:00 to 18:00 LT (local time) and minimum around 12:00 LT.

On the creation, depletion, and end of life of polar cap patches

Ionospheric convection patterns from the Super Dual Auroral Radar Network are used by Eriksen et al. (2023) to determine the trajectories, transit times, and decay rates of three polar cap patches from their creation in the dayside polar cap ionosphere to their end of life on the nightside (see Figure 4). The first two polar cap patches were created within 12 min of each other and travelled through the dayside convection throat, before entering the nightside auroral oval after 104 min and 92 min, respectively. When the patches approached the nightside auroral oval, an intensification in the poleward auroral boundary occurred close to their exit point, followed by a decrease in the transit velocity. The last patch (patch 3) decayed completely within the polar cap and had a lifetime of only 78 min. After a change in drift

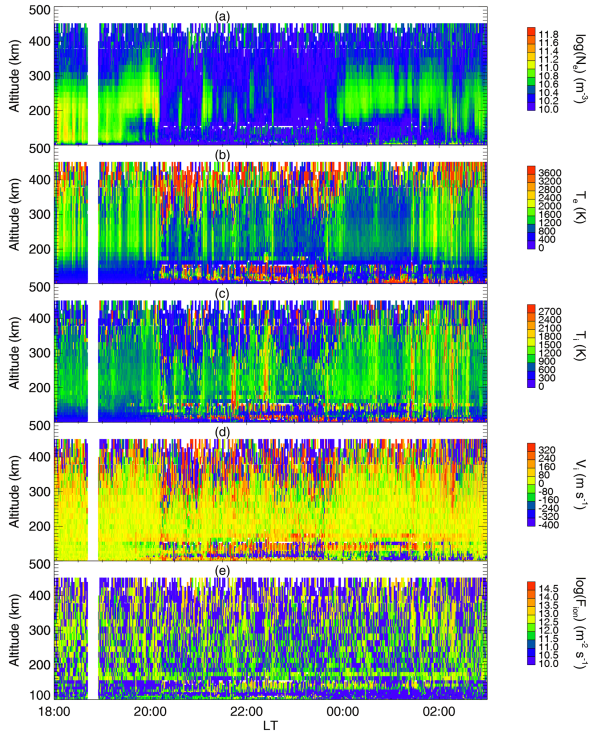

Figure 3: EISCAT Svalbard Radar (42 m dish) parameter plot for the nightside on 28 December 2007. The panels (a) to (e) are, respectively, the electron density, electron temperature, ion temperature, ion drift velocity and ion flux. The increased noise level is noted.

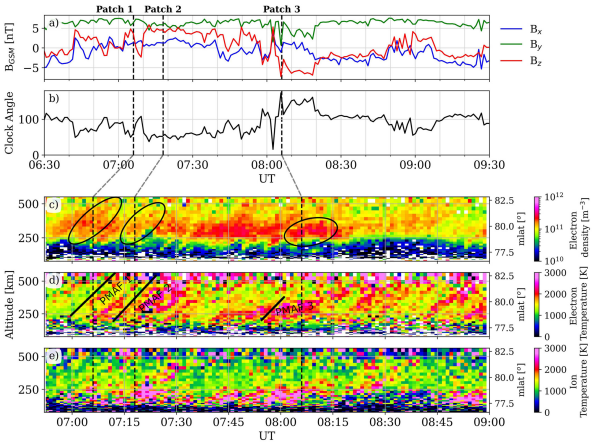

Figure 4: (a) Interplanetary magnetic field measurements from ACE and (b) shows corresponding clock angles on 19 December 2014. (c) shows EISCAT Svalbard Radar (ESR) 32 m electron number density, and (d) and (e) show ESR 32 m electron and ion temperatures, respectively. ESR measured at 30° elevation during this time period. Release times for patches 1, 2 and 3 are seen as vertical, dashed lines and their density signatures are circled. The poleward moving auroral forma are labeled, and their start time is represented by a black, tilted line.

direction, patch 3 had a radar backscatter power half-life of 4.23 min, which reduced to 1.80 min after a stagnation, indicating a variable decay rate. 28 min after the change in direction, and 16 min after coming to a halt within the Clyde River radar field-of-view, patch 3 appeared to reach its end of life. Eriksen et al. (2023) relate this rapid decay to increased frictional heating, which speeds up the recombination rate. Therefore, they suggest that the slowed patch motion within the polar cap convection pattern is a major factor in determining whether the patch survives as a recognizable density enhancement by the time the flux tubes comprising the initial patch cross into the nightside auroral oval.

Statistical comparison of electron precipitation during auroral breakups occurring either near the open-closed field line boundary or in the central part of the auroral oval

Auroral electron precipitation during a substorm exhibits complex spatiotemporal variations which are still not fully understood, especially during the very dynamic phase immediately following the onset. Since during disturbed times, the auroral oval typically extends across several hundreds of kilometres in the latitudinal direction, one may expect that precipitating electron spectra differ at locations close to the open-closed field line boundary (OCB) compared to the central part of the auroral oval. Grandin et al. (2024) carry out a statistical study based on 57 auroral breakups associated with substorm onsets observed above Tromsø (66.7°N geomagnetic latitude, i.e. central oval) and 25 onsets occurring above Svalbard (75.4°N geomagnetic latitude (see Figure 5), i.e. poleward boundary) between 2015 and 2022. The events were selected based on the availability of both optical observations and field-aligned incoherent scatter radar measurements. Those are two sets of different substorms; hence, we compare

solar wind driving conditions and geomagnetic indices for the two event lists in the statistical sense. Using the ELectron SPECtrum (ELSPEC) method (based on the inversion of the electron density profile) on the radar data, Grandin et al. (2024) retrieve precipitating electron fluxes within 1 keV to 100 keV around each onset time, and they apply the superposed epoch analysis method to the electron spectra at each location. They compare the statistical precipitation characteristics above both sites in terms of the peak differential flux, the energy of the peak, the integrated energy flux, and their time evolution during the minutes following the onset. They find that the integrated energy flux associated with events occurring in the central part of the auroral oval (Tromsø) exhibit a sharp peak of up to 25 mW m^{-2} in the first 2 min following the auroral breakup before decreasing and maintaining stable values of around 7 mW m^{-2} for at least 20 min. In turn, no initial peak is seen near the open-closed field line boundary (Svalbard), and values remain low throughout (1 mW m^{-2} to 2 mW m^{-2}). A comparison of the median spectra indicates that the precipitating flux of >10 keV electrons is lower above Svalbard than above Tromsø by a factor of at least 10, which may partly explain the differences. However, it proves difficult to conclude whether the differences originate from the latitude at which the auroral breakup takes place or from the fact that the breakups seen from Svalbard occur Equatorward from the radar beam, which only sees expansion-phase precipitation after a few minutes.

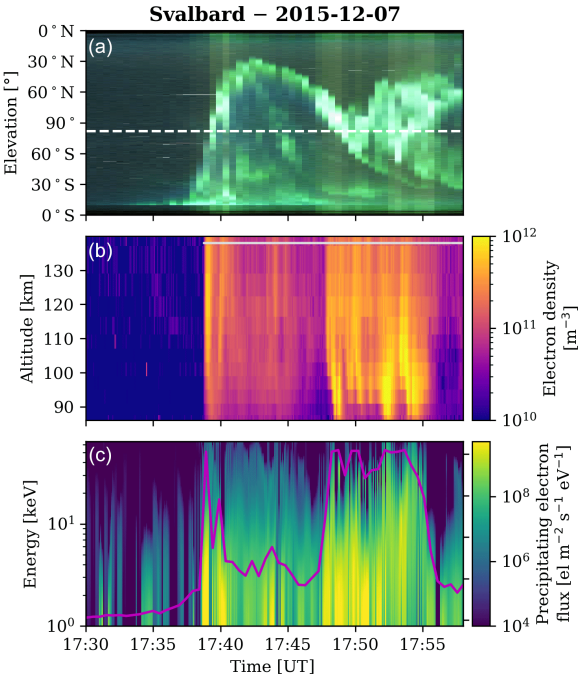

Figure 5: Example of auroral breakup observed above Svalbard on 7 December 2015. (a) Keogram from the Sony camera in Longyearbyen. The dashed white line indicates the elevation corresponding to the local magnetic field direction, ie the pointing direction of EISCAT Svalbard Radar (ESR). (b) Electron density profile measured by ESR. (c) Precipitating electron differential number flux derived with the ELSPEC method from the ESR measurements. The magenta line indicates the optical emission brightness (arbitrary unit, linearly scaled) within the ESR beam, ie along the dashed white line in panel (a). The small light-grey dots at the top of panel (b) indicate times with "valid" data points retained in the superposed epoch analysis for this event.

Influence of meteoric smoke particles on the incoherent scatter measured with EISCAT VHF

Meteoric ablation in the Earth's atmosphere produces particles of nanometer size and larger. These particles can become charged and influence the charge balance in the D region (60 km to 90 km) and the incoherent scatter observed with radar from there. Radar studies have shown that, if enough dust particles are charged, they can influence the received radar spectrum below 100 km, provided the electron density is sufficiently high (larger than 10^3 m^{-3}). Gunnarsdottir et al. (2024) studied an observation made with the EISCAT VHF radar on 9 January 2014 during strong particle precipitation so that incoherent scatter was observed down to almost 60 km altitude. They found that the measured spectra were too narrow in comparison to the calculated spectra. Adjusting the collision frequency provided a better fit in the frequency range of ±10 Hz to ±30 Hz. However, this did not lead to the best fit in all cases, especially not for the central part of the spectra in the narrow frequency range of ±10 Hz. By including a negatively charged dust component (see Figure 6), they obtained a better fit for spectra observed at altitudes of 75 km to 85 km, indicating that dust influences the incoherent-scatter spectrum at D-region altitudes. The observations at lower altitudes were limited by the small number of free electrons, and observations at higher altitudes were limited by the height resolution of the observations. Inferred dust number densities range from a few particles up to 10^4 cm^{-3}, and average sizes range from approxim-

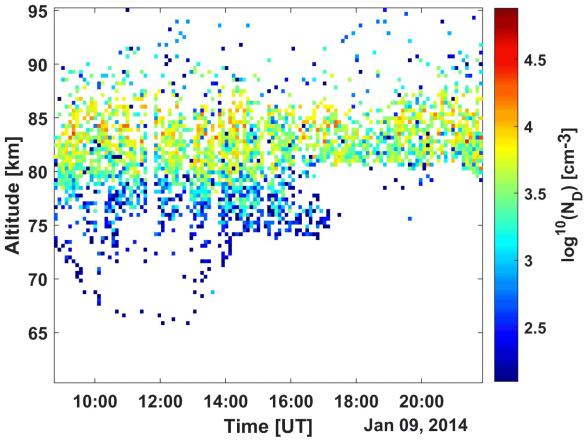

Figure 6: Derived number density (cm^{-3}) of negatively charged dust needed to fit to measured spectrum, shown for the time and altitude ranges of the observations.

ately 0.6 nm to 1 nm. They found an acceptable agreement with the dust profiles calculated with the WACCM-CARMA (Whole Atmosphere Community Climate Model-Community Aerosol Radiation Model for Atmospheres) model. However, these do not include charging, which is also based on models.

Inferring neutral winds in the ionospheric transition region from atmospheric-gravity-wave travelling-ionospheric-disturbance (AGW-TID) observations with the EISCAT VHF radar and the Nordic Meteor Radar Cluster

Atmospheric gravity waves and travelling ionospheric disturbances can be observed in the neutral atmosphere and the ionosphere at a wide range of spatial and temporal scales. Especially at medium scales, these oscillations are often not resolved in general circulation models and are parameterised. Günzkofer, Pokhotelov et al. (2023) show that ionospheric disturbances forced by upward-propagating atmospheric gravity waves can be simultaneously observed with the EISCAT very high frequency incoherent scatter radar and the Nordic Meteor Radar Cluster. From combined multi-static measurements, both vertical and horizontal wave parameters can be determined by applying a specially developed Fourier filter analysis method. This method is demonstrated using the example of a strongly pronounced wave mode

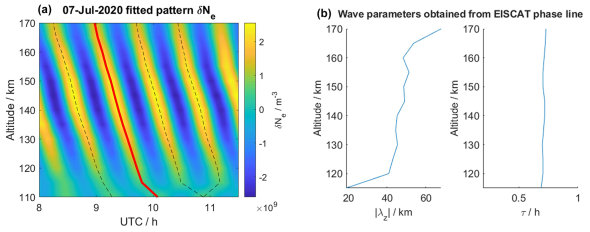

Figure 7: (a) Fitted wave pattern with phase lines (dashed). (b) Profiles of absolute vertical wavelength and wave period for the red phase line.

that occurred during the EISCAT experiment on 7 July 2020. Leveraging the developed technique, they show that the wave characteristics of travelling ionospheric disturbances are notably impacted by the fall transition of the mesosphere and lower thermosphere. They also demonstrate the application of using the determined wave parameters to infer the thermospheric neutral wind velocities. Applying the dissipative anelastic gravity wave dispersion relation, they obtain vertical wind profiles in the lower thermosphere.

On the factors controlling the relationship between type of pulsating aurora and energy of pulsating auroral electrons: Simultaneous observations by Arase satellite, ground-based all-sky imagers and EISCAT radar

Pulsating Aurora (PsA) is one of the major classes of diffuse aurora associated with precipitation of a few to a few tens of keV electrons from the magnetosphere. Recent studies suggested that, during PsA, more energetic (ie, subrelativistic/relativistic) electrons precipitate into the ionosphere at the same time. Those electrons are considered to be scattered at the higher latitude part of the magnetosphere by whistler-mode chorus waves propagating away from the magnetic equator. However, there have been no actual cases of simultaneous observations of precipitating electrons causing PsA (PsA electrons) and chorus waves propagating toward higher latitudes; thus, we still do not quite well understand under what conditions PsA electrons become harder and precipitate to lower altitudes. To address this question, Ito et al. (2024) have investigated an extended interval of PsA on 12 January 2021, during which simultaneous observations with the Arase satellite, ground-based all-sky imagers and the European Incoherent SCATter (EIS-

CAT) radar were conducted (see Figure 8). They found that, when the PsA shape became patchy, the PsA electron energy increased and Arase detected intense chorus waves at magnetic latitudes above 20°, indicating the propagation of chorus waves up to higher latitudes along the field line. A direct comparison between the irregularities of the magnetospheric electron density and the emission intensity of PsA patches at the footprint of the satellite suggests that the PsA morphology and the energy of PsA electrons are determined by the presence of "magnetospheric density ducts", which allow chorus waves to travel to higher latitudes and thereby precipitate more energetic electrons.

Do the throat auroras create polar cap patches?

Throat auroras and polar cap patches are common phenomena in the polar ionosphere resulting from magnetosphere-ionosphere coupling. D. Zhang et al. (2023) reports from a campaign, with all-sky imagers at Yellow River Station, the European Incoherent Scatter Svalbard Radar, and coordinated low-altitude spacecraft observations. During periods of radial interplanetary magnetic field (IMF), observations showed that, as poleward moving throat auroras faded around the polar cap boundary, they linked to poleward moving ionization patches (see Fiugure 9). The throat auroras were produced by soft-electron precipitation associated with dayside magnetic reconnection. The red line emission intensity of throat auroras was correlated with dayside reconnection events. Dense plasma from lower latitudes was transported poleward via enhanced convection in the throat auroras to form patches. This is a potentially new formation mechanism for patches associated with throat auroras and magnetic reconnection for radial IMF. Moreover, the patches move anti-sunward due to the $\vec{E} \times \vec{B}$ drift.

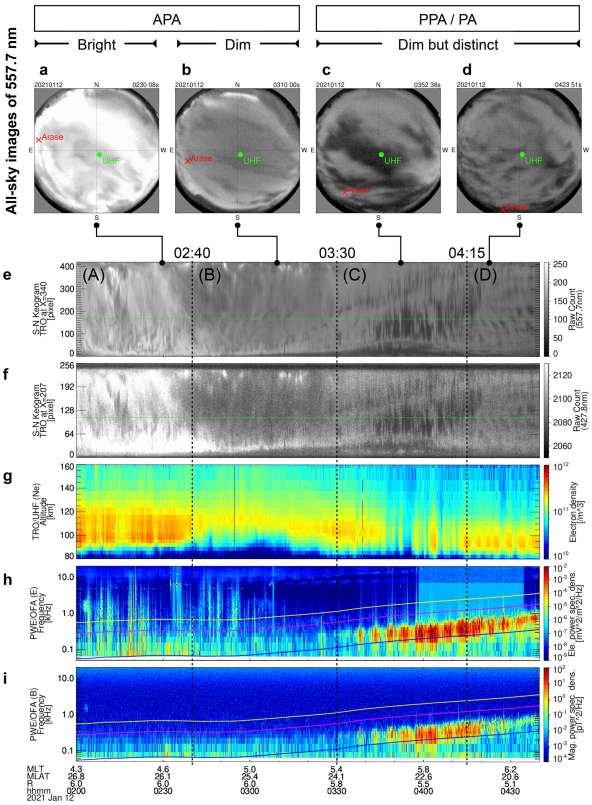

Figure 8: Overview of the simultaneous observations during 02:00-04:40 UT on 12 January 2021, where four time periods were defined by considering the transition of PsA morphology; (A): 02:00-02:40 UT, (B): 02:40-03:30 UT, (C): 03:30-04:15 UT, and (D): 04:15–04:40 UT. Magnetic Latitude (MLAT) and R indicate the position of the Arase satellite in the magnetosphere. (a–d) Representative all-sky images from the four time periods respectively taken at 02:30:08, 03:10:00, 03:52:38, and 04:23:51 UT with the Watec all-sky imager. (e, f) Time-series of the optical intensity along the south-to-north cross-section (keogram), including the beam direction of EISCAT denoted by the horizontal green line. (g) Altitude-time plot of the electron density (ionization profile) obtained from the EISCAT radar. (h, i) Frequency-time diagrams of electric and magnetic field's power spectral density observed by PWE/OFA on board Arase, where the three horizontal yellow, red and blue curves represent f_{ce}, $0.5f_{ce}$ and $0.1fce$, at the magnetic equator estimated by the TS05 model, respectively.

On mechanisms for high-frequency pump-enhanced optical emissions at 557.7 nm and 630.0 nm from atomic oxygen in the high-latitude F-region ionosphere

Leyser et al. (2023) reported from an experiment where the EISCAT (European Incoherent Scatter Scientific Association) Heating facility was used to transmit powerful high-frequency (HF) electromagnetic waves into the F-region ionosphere to enhance optical emissions at 557.7 nm and 630.0 nm from atomic oxygen. The emissions were imaged by several stations of ALIS (Auroral Large Imaging System) in northern Sweden, and the EISCAT UHF incoherent scatter radar was used to obtain plasma parameter values. The ratio of

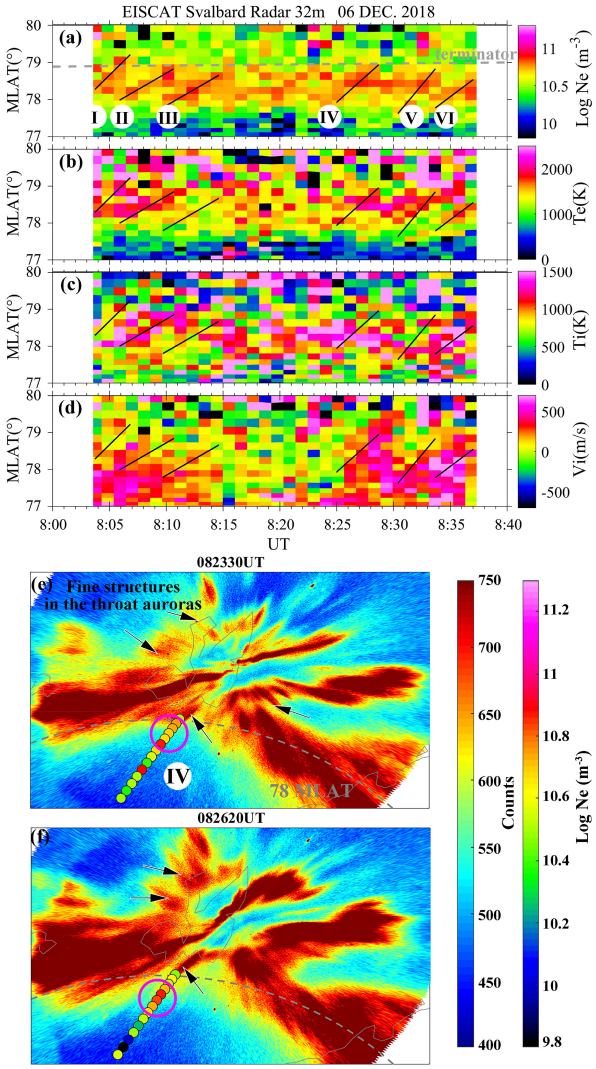

Figure 9: (a) Electron density, (b and c) ion and electron temperatures, and (d) ion line-of-sight velocity observed by the EISCAT Svalbard Radar (ESR) 32 m. Positive velocities are away from the radar. The dashed gray line highlights the terminator location along the geomagnetic longitude of Longyearbyen (∼111°E) at 300 km. (e and f) The 630.0 nm YRS ASI overlaid with ESR 32 m electron density observations plotted in magnetic local time-magnetic latitude coordinates at 082330 UT and 082620 UT. The black arrows with white borders highlight some fine-structures in the throat auroras. The magenta circles highlight patch "IV".

the 557.7 nm to 630.0 nm column emission rates changed from $I_{5577}/I_{6300} \approx 0.2$ for the HF pump frequency $f_0 = 6.200\,\mathrm{MHz} \approx 4.6 f_e$ to $I_{5577}/I_{6300} \approx 0.5$ when $f_0 = 5.423\,\mathrm{MHz} \lesssim 4 f_e$, where f_e is the ionospheric electron gyro frequency (see Figure 10). The observations are interpreted in terms of decreased electron heating efficiency and

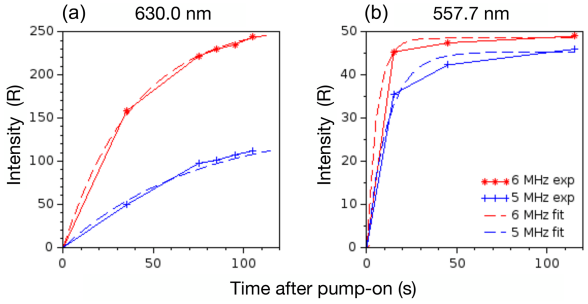

Figure 10: Temporal evolution of the pump-enhanced column emission rates at 630.0 nm (a) and 557.7 nm (b) after pump-on time at time $t = 0$ s. The solid lines connect the data points shown by markers (red * symbols for $f_0 = 6.200$ MHz and blue + symbols for $f_0 = 5.423$ MHz). The dashed lines are fits with observed emission growth times.

thereby weaker enhancement at 630.0 nm for $f_0 = 5.423\,\mathrm{MHz} \lesssim 4 f_e$. The emissions at 557.7 nm are attributed to electron acceleration by upper hybrid waves of metre-scale wavelengths that can be excited with $f_0 = 5.423\,\mathrm{MHz} \lesssim 4 f_e$.

Atmospheric ionizations by solar X-Rays, solar protons, and radiation belt electrons in September 2017 space weather event

Energetic particles from space deposit their energies on the Earth's atmosphere and contribute to variations in the concentration of neutral components such as ozone which controls the atmospheric temperature balance. Comprehensive understandings of their global impact on the atmosphere require whole pictures of spatiotemporal ionization distributions due to them. Murase et al. (2023) first attempted to evaluate and summarize the altitude profiles of ionization for the September 2017 space weather event with cutting-edge space-borne and ground-based observations of different types of particle inputs. In early September 2017, the Sun showed notable activity, including X-class flares and solar proton events. During this period, ground-based radar observations have confirmed atmospheric ionization events by energetic particle precipitations of solar flare X-rays, solar protons, and radiation belt electrons, the main sources of ionization into the Earth's atmosphere. They estimated the altitude profiles of the ionization rate by using the Particle and Heavy Ion Transport code System (PHITS) with the input of the particle fluxes obtained by satellites.

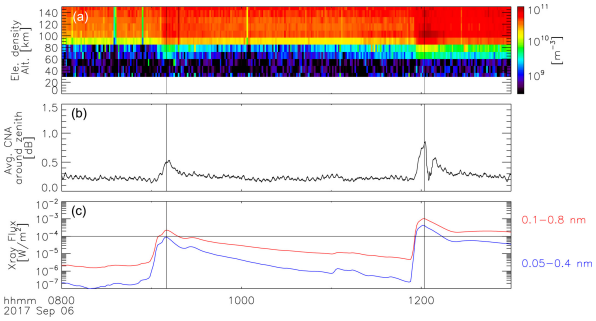

Figure 11: Ground-based and satellite measurements during two X-class solar flares on 6 September 2017. (a) Electron density by the EISCAT radar at Tromsø and (b) CNA at Syowa Station and (c) X-ray fluxes by the GOES-15 satellite are shown. A horizontal black line in panel (c) represents a flux of 104 W/m^2, and flares with fluxes exceeding this at 0.1 nm to 0.8 nm are classified as X-class. Vertical lines indicate two peaks of X-ray fluxes at 0910 UT and 1202 UT.

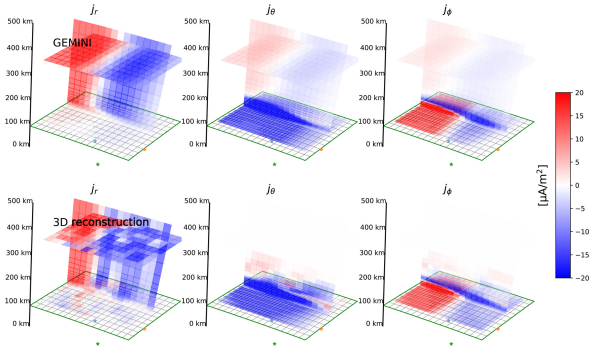

Figure 12: Example of how the proposed volumetric reconstruction technique performs shown on a vertical north-south slice through the domain, and two horizontal cuts at 102.5 km and 355 km altitude. Top row: The ground truth that is sampled from (GEMINI model with no noise). The three columns show the r, θ, and ϕ components of the full 3D current density vector. Bottom row: the corresponding estimated values from the volumetric reconstruction described above. Reconstruction of the horizontal components is overall better than the reconstruction of the radial component.

The estimates are then compared with measurements of the ionization altitude, ionization intensity, and electron density by the radars in the polar region, such as the PANSY radar at Syowa Station and the EISCAT in Tromsø, Norway (see Figure 11). They concluded that the PHITS simulation results reasonably reproduce (within the error of a factor of two) those ionizations measured by ground-based instruments with inputs of observed ionization sources by satellites.

Volumetric Reconstruction of Ionospheric Electric Currents From Tri-Static Incoherent Scatter Radar Measurements

Reistad et al. (2024) presented a new technique for the upcoming tri-static incoherent scatter radar system EISCAT_3D (E3D) to perform a volumetric reconstruction of the 3D ionospheric electric current density vector field, focusing on the feasibility of the E3D system. The input to their volumetric reconstruction technique are estimates of the 3D current density perpendicular to the main magnetic field, $\vec{j}_\perp$, and its covariance, to be obtained from E3D observations based on two main assumptions: (a) Ions fully magnetized above the E region, set to 200 km here. (b) Electrons fully magnetized above the base of the domain, set to 90 km. In this way, $\vec{j}_\perp$ estimates are obtained without assumptions about the neutral wind field, allowing it to be subsequently determined. The volumetric reconstruction of the full 3D current density is implemented as vertically coupled horizontal layers represented by Spherical Elementary Current Systems with a built-in current continuity constraint. They demonstrated that their technique is able to retrieve the three dimensional nature of the currents in their idealized setup, taken from a simulation of an active auroral ionosphere using the Geospace Environment Model of Ion-Neutral Interactions (GEMINI) (see Figure 12). The vertical current is typically less constrained than the horizontal, but they outlined strategies for improvement by utilizing additional data sources in the inversion. The ability to reconstruct the neutral wind field perpendicular to the magnetic field in the E region was demonstrated to mostly be within ±50 m s^{-1} in a limited region above the radar system in their setup.

The first simultaneous spectroscopic and monochromatic imaging observations of short-wavelength infrared aurora of N_2^+ Meinel (0,0) band at 1.1 μm with incoherent scatter radar

A study by Nishiyama et al. (2024) presents a first simultaneous observation of N_2^+ Meinel (0,0) band (hereafter, N_2^+ (M)) aurora by cutting-edge short-wavelength infrared imaging spectrograph (NIRAS-2) and monochromatic camera

(NIRAC) installed at the Kjell Henriksen Observatory (78°N, 16°E). On January 21 2023, N_2^+ (M) intensification that is associated with a band-shape aurora structure was observed by the NIRAS-2 and the NIRAC having temporal resolutions of 30 s and 20 s, respectively. In addition, the European incoherent scatter Svalbard Radar also observed electron density variations at the same time (see Figure 13). Electron density measured at altitude range from 100 km to 120 km shows similar variations as of N_2^+ (M) intensity, which implies that a primary source of N_2^+ (M)) emissions is direct collisions of N_2 by precipitating electrons penetrating down to around 100 km altitude (up to 10 keV). However, the observation also demonstrated moderate correlations between N_2^+ (M) intensity and electron density above 140 km, which implies that different N_2^+ (M) generation process, N_2 charge exchange with O^+, may work up to near 160 km and make a non-negligible contribution to N_2^+ (M) emissions. This hypothesis would be verified with further radar observations or stereo imaging observations useful to estimate the vertical distribution of the emission layers. The N_2^+ (M) is a very promising target wavelength for aurora observation because the quality of sensors is highly expected to improve further and further. Continuous observations with their new instruments will undoubtedly provide an important information of N_2^+ (M) characteristics, for future missions of both balloon-borne and satellite-borne imaging.

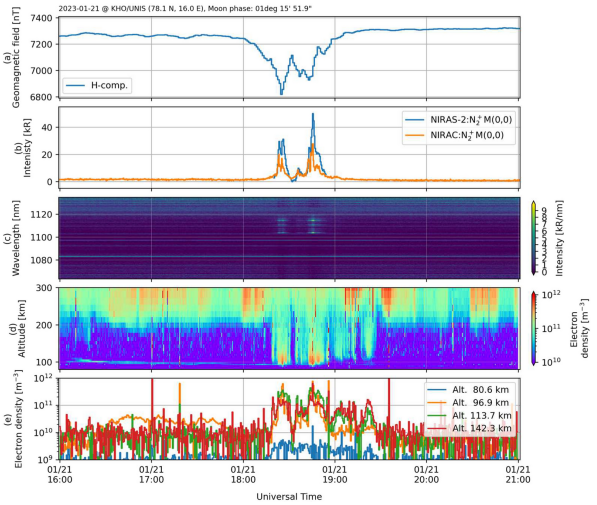

Figure 13: Summary plots for temporal evolution of the observed N_2^+ (M) with ionospheric variations. (a) H-component of geomagnetic fields, (b) N_2^+ (M) intensity observed by the NIRAS-2 and the NIRAC, (c) dynamic spectrum from 1065 nm to 1135 nm obtained by the NIRAS-2, (d) electron density along the field line as functions of altitude and time, and (e) electron density variations for the four different altitudes along the field line observed by the EISCAT Svalbard Radar.

Ionospheric fireworks illuminate auroral science

Sergienko et al. (2024) report that in March 2023, reindeer out for an evening snack on the Scandinavian tundra, as well as other nighttime observers, saw an unusual display of bright purple and green clouds intersecting an auroral display in an otherwise clear sky (see Figure 14). Nature provided the aurora, but the clouds were courtesy of a sounding rocket that released barium into the atmosphere to help reveal the electrodynamics near the aurora. The electrodynamics of the auroral ionosphere give us important information about space weather that can affect the operation of satellites, power lines, and more. The Barium Release Optical and Radio rocket (BROR) was launched at 19:23 local time (18:23 UTC) on 23 March 2023 from the Esrange Space Center in northern Sweden. Observations of the background ionosphere were collected with the European Incoherent Scatter (EISCAT) radar system during BROR provided the parameters of the ambient ionosphere, such as electron density and electron and ion temperatures.

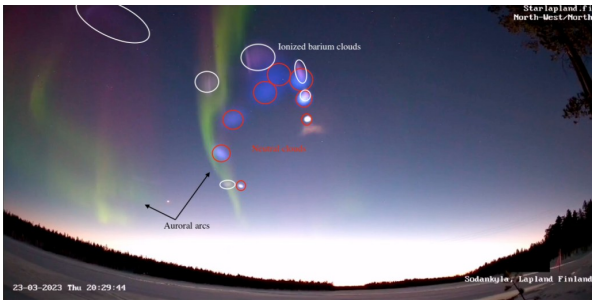

Figure 14: Barium clouds and auroral arcs are seen in this still frame from a video shot from Sodankylä, Finland, with a digital camera at 18:29:44 UTC, 15 s after the last barium release of the Barium Release Optical and Radio rocket experiment on 23 March 2023. Neutral (red ovals) and ionized (white ovals) barium clouds as well as auroral arcs are indicated in the annotated video still. Credit: Starlapland/Samuli Korvanen

Application of generalised-aurora computed tomography to the EISCAT_3D project

EISCAT_3D is a project to build a multi-site phased-array incoherent scatter radar system in northern Fenno-Scandinavia. Tanaka et al. (2024) demonstrated via numerical simulation how useful monochromatic images taken by a multi-point imager network are for auroral research in the EISCAT_3D project. They applied the generalised aurora computed tomography (G-ACT) method to modelled observational data from real instruments, such as the Auroral Large Imaging System (ALIS) and the EISCAT_3D radar (see Figure 15). G-ACT is a method for reconstructing the three-dimensional (3D) distribution of auroral emissions and ionospheric electron density (corresponding to the horizontal two-dimensional (2D) distribution of energy spectra of precipitating electrons) from multi-instrument data. It is assumed that the EISCAT_3D radar scans an area of 0.8° in geographic latitude and 3° in longitude at an altitude of 130 km with 1010 beams from the radar core site at Skibotn (69.35°N, 20.37°E). Two neighbouring discrete arcs were assumed to appear in the observation region of the EISCAT_3D radar. The reconstruction results from G-ACT were compared with those from the normal ACT as well as the ionospheric electron density from the radar. It was found that G-ACT can interpolate the ionospheric electron density at a much higher spatial resolution than that observed by the EISCAT_3D radar. Furthermore, the multiple arcs reconstructed by G-ACT are more precise than those by ACT. In particular, underestimation of the ionospheric electron density and precipitating electrons' energy fluxes inside the arcs is significantly improved by G-ACT including the EISCAT_3D data. Even when the ACT reconstruction is difficult due to the unsuitable locations of the imager sites relative to the discrete arcs and/or a small number of available images, G-ACT allows for obtaining better reconstruction results.

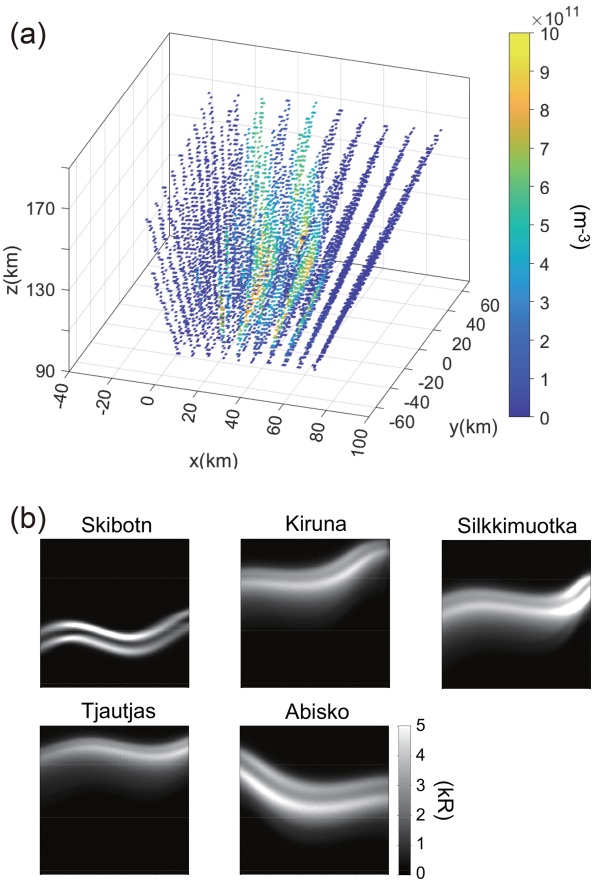

Figure 15: (a) Modelled ionospheric electron density data obtained by the EISCAT_3D radar. (b) Modelled auroral images taken at five ALIS stations. Top and right of the images correspond to the north-ward and west-ward directions, respectively.

The high latitude ionospheric response to the major May 2024 geomagnetic storm: a synoptic view

The high latitude ionospheric evolution of the May 10–11, 2024, geomagnetic storm was investigated by Themens et al. (2024) in terms of Total Electron Content (TEC) and contextualized with Incoherent Scatter Radar (ISR) and ionosonde observations. Substantial plasma lifting was observed within the initial storm enhanced density plume with ionospheric peak heights increasing by 150 km to 300 km, reaching levels of up to 630 km. Scintillation was observed within the cusp during the initial expansion phase of the storm, spreading across the auroral oval thereafter. Patch transport into the polar cap produces broad regions of scintillation that were rapidly cleared from the region after a strong Interplanetary Magnetic Field (IMF) reversal at 223 UT. Strong heating and composition changes resulted in the complete absence of the F2-layer on the eleventh, suffocating high latitude convection from dense plasma necessary for tongue of ionization and patch formation, ultimately resulting in a suppression of polar cap scintillation on the eleventh.

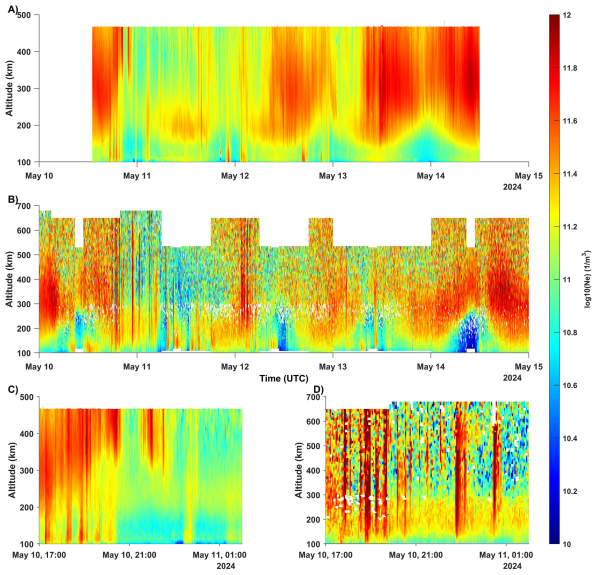

Figure 16: The electron density over the EISCAT Svalbard Radar (ESR) (A), over PFISR (B) for the 10–14 May with zoomed in periods between 17 UT on May 10 and 02 UT on May 11 for ESR (C) and PFISR (D). These show the disappearance of the F2 layer with plasma densities an order of magnitude lower in the 11th compared to pre-storm conditions.

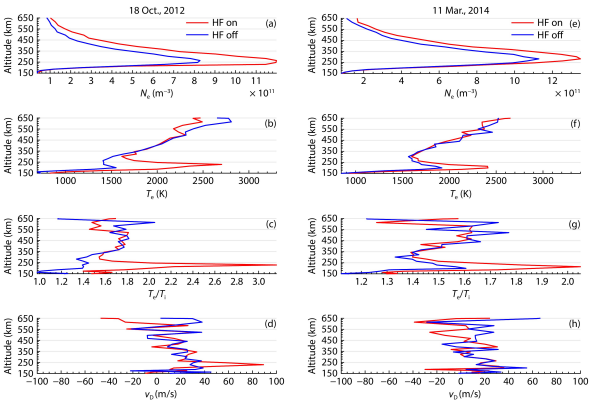

Figure 17: (a) Mean electron density; (b) mean electron temperature; (c) mean ratio of electron temperature to ion temperature; and (d) mean ion drift velocity measured in one Heating experiment. Each enhanced (red) or background (blue) value is the mean of the integration of the X mode pump wave, over the final 60 s of the on/off period, for five cycles. Subplots (e), (f), (g), and (h) correspond to (a), (b), (c), and (d), respectively, for another Heating Experiment, and the description follows that of the first experiment but measured over only three on/off cycles.

The nature of electron density enhancement over a wide altitude range during ionosphere heating experiments at EISCAT

During the course of ionospheric heating experiments, researchers at the European Incoherent Scatter Scientific Association (EISCAT) observed an apparent electron density enhancement (see Figure 17). The enhancement extended over a wide range of altitudes, above the reflection altitude of the high-frequency pump wave. However, whether this enhancement actually corresponds to a true enhancement in electron density remains an open question. When the dispersion relation of ion acoustic waves is followed, the frequency ratio of the enhanced ion line to the background ion line suggests that the profile of the effective ion mass may have remained unchanged. Furthermore, the solar radio flux and ion drift velocity indicate no significant changes in the ion species and their densities. Hence, Wu et al. (2024) conclude that the electron density enhancement observed at EISCAT should not, in fact, be considered a true enhancement.

Publications 2023–2024

Akhmetov, O. I., Mingalev, I. V., Mingalev, O. V., Belakhovsky, V. B., & Suvorova, Z. V. (2023). Features of radio signal propagation in the VLF range at high latitudes during solar proton events. *Geomagnetism and Aeronomy*, *63*(4), 367–376. https://doi.org/10.1134/s0016793223600108

Baddeley, L., Lorentzen, D., Haaland, S., Heino, E., Mann, I., Miloch, W., Oksavik, K., Partamies, N., Spicher, A., & Vierinen, J. (2023). Space and atmospheric physics on Svalbard: A case for continued incoherent scatter radar measurements under the cusp and in the polar cap boundary region. *Progress in Earth and Planetary Science*, *10*(1), 53. https://doi.org/10.1186/s40645-023-00585-9

Bag, T., & Ogawa, Y. (2024a). Impact of interplanetary shock on nitric oxide cooling emission: A superposed epoch study. *Advances in Space Research*, *74*(11), 6012–6019. https://doi.org/10.1016/j.asr.2024.08.005

Bag, T., & Ogawa, Y. (2024b). Response time of Joule heating rate and nitric oxide cooling emission during geomagnetic storms: Correlated ground-based and satellite observations. *Journal of Geophysical Research: Space Physics*, *129*(2), e2023JA032072. https://doi.org/10.1029/2023ja032072

Bag, T., Ogawa, Y., & Sivakumar, V. (2024). Thermospheric NO cooling during 2003 October "Halloween Storm": Revisited. *Journal of Geophysical Research: Space Physics*, *129*(7), e2024JA032805. https://doi.org/10.1029/2024ja032805

Bag, T., & Ogawa, Y. (2024c). Enhanced response of thermospheric cooling emission to negative pressure pulse. *Scientific Reports*, *14*(1), 9647. https://doi.org/10.1038/s41598-024-60471-2

Bag, T., Sivakumar, V., & Ogawa, Y. (2024). Impact of interplanetary shock on thermospheric cooling emission: A case study. *Journal of Geophysical Research: Space Physics*, *129*(10), e2024JA033176. https://doi.org/10.1029/2024ja033176

Baloukidis, D., Sarris, T., Tourgaidis, S., Pirnaris, P., Aikio, A., Virtanen, I., Buchert, S., & Papadakis, K. (2023). A comparative assessment of the distribution of Joule heating in altitude as estimated in TIE-GCM and EISCAT over one Solar cycle. *Journal of Geophysical Research: Space Physics*, *128*(12), e2023JA031526. https://doi.org/10.1029/2023ja031526

Belakhovsky, V. B., Vasilev, A. E., Kalishin, A. S., & Roldugin, A. V. (2024). Disturbances of GLONASS/GPS signals during a magnetic storm on March 23–24, 2023, according to observations at the Kola peninsula. *Bulletin of the Russian Academy of Sciences: Physics*, *88*(3), 359–367. https://doi.org/10.1134/s1062873823705524

Blagoveshchenskaya, N. F., Kalishin, A. S., Borisova, T. D., Egorov, I. M., & Zagorskiy, G. A. (2023). Phenomena in the high-latitude F region of the ionosphere under the effect of powerful HF radio waves at frequencies above the critical one of the F2 layer. *Geomagnetism and Aeronomy*, *63*(6), 757–769. https://doi.org/10.1134/s0016793223600467

Blagoveshchenskaya, N. F., Borisova, T. D., Kalishin, A. S., & Egorov, I. M. (2023). Artificial ducts created via high-power HF radio waves at EISCAT. *Remote Sensing*, *15*(9), 2300. https://doi.org/10.3390/rs15092300

Borisova, T., Blagoveshchenskaya, N., & Kalishin, A. (2023a). Features of artificial ionosphere turbulence induced by the O- and X-mode HF heating near the F2-layer critical frequency. *Solar-Terrestrial Physics*, *9*(1), 21–30. https://doi.org/10.12737/stp-91202303

Borisova, T., Blagoveshchenskaya, N., & Kalishin, A. (2023b). Spectral features of ionospheric plasma waves excited by powerful HF radio waves radiated at frequencies near electron gyroharmon-

ics and F2-layer critical frequency. *Solar-Terrestrial Physics*, *9*(2), 94–102. https://doi.org/10.12737/stp-92202312

Borisova, T., Blagoveshchenskaya, N., Kalishin, A., & Kovalev, A. (2024). Determination of the vector velocity of artificial ionospheric irregularities based on Doppler measurements by the bi-static scatter method of HF radio signals propagating over long radio paths. *Solar-Terrestrial Physics*, *10*(2), 74–92. https://doi.org/10.12737/stp-102202408

Borries, C., Iochem, P., Tasnim, S., & Davis, F. (2024). Persistent high-latitude ionospheric response to solar wind forcing. *Journal of Space Weather and Space Climate*, *14*, 33. https://doi.org/10.1051/swsc/2024029

Cai, L., Aikio, A., Oyama, S., Ivchenko, N., Vanhamäki, H., Virtanen, I., Buchert, S., Mekuriaw, M. L., & Zhang, Y. (2024). Effect of polar cap patches on the high-latitude upper thermospheric winds. *Journal of Geophysical Research: Space Physics*, *129*(8), e2024JA032819. https://doi.org/10.1029/2024ja032819

Carter, J. A., Dunlop, M., Forsyth, C., Oksavik, K., Donovon, E., Kavanagh, A., Milan, S. E., Sergienko, T., Fear, R. C., Sibeck, D. G., Connors, M., Yeoman, T., Tan, X., Taylor, M. G. G. T., McWilliams, K., Gjerloev, J., Barnes, R., Billet, D. D., Chisham, G., … Zhang, Q.-H. (2024). Ground-based and additional science support for SMILE. *Earth and Planetary Physics*, *8*(1), 275–298. https://doi.org/10.26464/epp2023055

Collinson, G. A., Glocer, A., Pfaff, R., Barjatya, A., Conway, R., Breneman, A., Clemmons, J., Eparvier, F., Michell, R., Mitchell, D., Imber, S., Akbari, H., Davis, L., Kavanagh, A., Robertson, E., Swanson, D., Xu, S., Miller, J., Cameron, T., … Zesta, E. (2024). Earth's ambipolar electrostatic field and its role in ion escape to space. *Nature*, *632*(8027), 1021–1025. https://doi.org/10.1038/s41586-024-07480-3

David, T. W., Michael, C. M., Wright, D., Talabi, A. T., & Ajetunmobi, A. E. (2024). Ionospheric upwelling and the level of associated noise at solar minimum. *Annales Geophysicae*, *42*(2), 349–354. https://doi.org/10.5194/angeo-42-349-2024

Domben, E. S., Sharma, P., & Mann, I. (2023). Using deep learning methods for segmenting polar mesospheric summer echoes. *Remote Sensing*, *15*(17), 4291. https://doi.org/10.3390/rs15174291

Ellahouny, N. M., Aikio, A. T., Vanhamäki, H., Virtanen, I. I., Cai, L., Marchaudon, A., Blelly, P.-L., Coster, A., Norberg, J., Maute, A., & Oyama, S.-I. (2024). EISCAT observations of depleted high-latitude F-region during an HSS/SIR-driven magnetic storm. *Journal of Geophysical Research: Space Physics*, *129*(9), e2024JA032910. https://doi.org/10.1029/2024ja032910

Eriksen, N. K., Lorentzen, D. A., Oksavik, K., Baddeley, L., Hosokawa, K., Shiokawa, K., Bland, E., Paxton, L., Zhang, Y., McWilliams, K., Yeoman, T., & Themens, D. R. (2023). On the creation, depletion, and end of life of polar cap patches. *Journal of Geophysical Research: Space Physics*, *128*(12), e2023JA031739. https://doi.org/10.1029/2023ja031739

ESA-NASA Lower Thermosphere-Ionosphere Science Working Group. (2024, July). *Exploring Earth's interface with space — The scientific case for a satellite mission to the lower thermosphere-ionosphere transition region* (ESA-EOPSM-ELTI-RP-4592). ESA. https://doi.org/10.5270/esa-nasa.lti-sc.2024-07-v1.0

Feng, T., Liu, M., He, S., Wang, X., & Zhou, C. (2024). Overshoot phenomena: Observation and simulation. *Earth and Planetary Physics*, *8*(2), 1–9. https://doi.org/10.26464/epp2024010

Frøystein, I., Spicher, A., Gustavsson, B., Oksavik, K., & Johnsen, M. G. (2024). On the identification of the dayside auroral region using incoherent scatter radar. *Journal of Geophysical Research: Space Physics*, *129*(12), e2024JA033361. https://doi.org/10.1029/2024ja033361

Geethakumari, G. P., Aikio, A. T., Cai, L., Vanhamäki, H., Virtanen, I. I., Coster, A., Marchaudon, A., Blelly, P.-L., Maute, A., Norberg, J., Oyama, S., Zhang, Y., & Kunduri, B. S. R. (2024). Total electron content variations during an HSS/SIR-driven geomagnetic storm at high and mid latitudes. *Journal of Geophysical Research: Space Physics*, *129*(12), e2024JA033192. https://doi.org/10.1029/2024ja033192

Grandin, M., Partamies, N., & Virtanen, I. I. (2024). Statistical comparison of electron precipitation during auroral breakups occurring either near the open–closed field line boundary or in the central part of the auroral oval. *Annales Geophysicae*, *42*(2), 355–369. https://doi.org/10.5194/angeo-42-355-2024

Gunnarsdottir, T. L., Mann, I., Feng, W., Huyghebaert, D. R., Haeggstroem, I., Ogawa, Y., Saito, N., Nozawa, S., & Kawahara, T. D. (2024). Influence of meteoric smoke particles on the incoherent scatter measured with EISCAT VHF. *Annales Geophysicae*, *42*(1), 213–228. https://doi.org/10.5194/angeo-42-213-2024

Gunnarsdottir, T. L., Poggenpohl, A., Mann, I., Mahmoudian, A., Dalin, P., Haeggstroem, I., & Rietveld, M. (2023). Modulation of polar mesospheric summer echoes (PMSEs) with high-frequency heating during low solar illumination. *Annales Geophysicae*, *41*(1), 93–114. https://doi.org/10.5194/angeo-41-93-2023

Gunnarsdottir, T. L. (2023, August). *Mesospheric dust — radar applications for detection and investigation* [PhD Thesis]. UiT The Arctic University of Norway. https://hdl.handle.net/10037/31666

Günzkofer, F., Liu, H., Stober, G., Pokhotelov, D., & Borries, C. (2024). Evaluation of the empirical scaling factor of Joule heating rates in TIE-GCM with EISCAT measurements. *Earth and Space Science*, *11*(4), e2023EA003447. https://doi.org/10.1029/2023ea003447

Günzkofer, F., Pokhotelov, D., Stober, G., Mann, I., Vadas, S. L., Becker, E., Tjulin, A., Kozlovsky, A., Tsutsumi, M., Gulbrandsen, N., Nozawa, S., Lester, M., Belova, E., Kero, J., Mitchell, N. J., & Borries, C. (2023). Inferring neutral winds in the ionospheric transition region from atmospheric-gravity-wave traveling-ionospheric-disturbance (AGW-TID) observations with the EISCAT VHF radar and the Nordic Meteor Radar Cluster. *Annales Geophysicae*, *41*(2), 409–428. https://doi.org/10.5194/angeo-41-409-2023

Günzkofer, F., Stober, G., Pokhotelov, D., Miyoshi, Y., & Borries, C. (2023). Difference spectrum fitting of the ion–neutral collision frequency from dual-frequency EISCAT measurements. *Atmospheric Measurement Techniques*, *16*(23), 5897–5907. https://doi.org/10.5194/amt-16-5897-2023

Haaland, S., Radlwimmer, A., van Schaik, B., Schillings, A., & Bjoland, L. (2023). Seasonal asymmetries and long-term trends in atmospheric and ionospheric temperatures in polar regions and their dependence on solar activity (SATS). In M. Gevers, D. T. David, R. C. Thakur, C. Hübner & J. Jania (Eds.), *The State of Environmental Science in Svalbard (SESS) report 2022*. Svalbard Integrated Arctic Earth Observing System. https://doi.org/10.5281/ZENODO.7371477

Hestad, T., Barabash, V., & Laufer, R. (2023). The APTAS student CubeSat mission: A case study for reflective practitioner in education and student teams. *Advances in Space Research*, *72*(6), 2245–2258. https://doi.org/10.1016/j.asr.2023.06.024

Hosokawa, K., Oyama, S.-I., Ogawa, Y., Miyoshi, Y., Kurita, S., Teramoto, M., Nozawa, S., Kawabata, T., Kawamura, Y., Tanaka, Y.-M., Miyaoka, H., Kataoka, R., Shiokawa, K., Brändström, U., Turunen, E., Raita, T., Johnsen, M. G., Hall, C., Hampton, D., … Fujii, R. (2023). A ground-based instrument suite for integrated high-time resolution measurements of pulsating aurora with Arase. *Journal of Geophysical Research: Space Physics*, *128*(8), e2023JA031527. https://doi.org/10.1029/2023ja031527

Ito, Y., Hosokawa, K., Ogawa, Y., Miyoshi, Y., Tsuchiya, F., Fukizawa, M., Kasaba, Y., Kazama, Y., Oyama, S., Murase, K., Nakamura, S., Kasahara, Y., Matsuda, S., Kasahara, S., Hori, T., Yokota, S., Keika, K., Matsuoka, A., Teramoto, M., & Shinohara, I. (2024). On the factors controlling the relationship between type of pulsating aurora and energy of pulsating auroral electrons: Simultaneous observations by Arase satellite, ground-based all-sky imagers and EISCAT radar. *Journal of Geophysical Research: Space Physics*, *129*(7), e2024JA032617. https://doi.org/10.1029/2024ja032617

Jee, G., Ji, E.-Y., Kim, E., Kwak, Y.-S., Lee, C., Kwon, H.-J., Kim, J.-E., Ham, Y.-B., Lee, J.-H., Kim, J.-H., Yang, T.-Y., & Kam, H. (2023). Observations for the ionosphere using European incoherent scatter (EISCAT) in the dayside polar cap/cusp and auroral region. *Journal of Astronomy and Space Sciences*, *40*(1), 1–10. https://doi.org/10.5140/jass.2023.40.1.1

Ji, E.-Y., Moon, Y.-J., Kwak, Y.-S., Yi, K., & Kim, J.-H. (2024). Construction of global IGS-3D electron density (N_e) model by deep learning. *Journal of Atmospheric and Solar-Terrestrial Physics*, *265*, 106370. https://doi.org/10.1016/j.jastp.2024.106370

Jin, Y., Moen, J. I., Spicher, A., Liu, J., Clausen, L. B. N., & Miloch, W. J. (2023). Ionospheric flow vortex induced by the sudden decrease in the Solar wind dynamic pressure. *Journal of Geophysical Research: Space Physics*, *128*(11), e2023JA031690. https://doi.org/10.1029/2023ja031690

Jozwicki, D., Sharma, P., Huyghebaert, D., & Mann, I. (2024). Polar mesospheric summer echo (PMSE) multilayer properties during the solar maximum and solar minimum. *Annales Geophysicae*, *42*(2), 431–453. https://doi.org/10.5194/angeo-42-431-2024

Kalishin, A. S., Blagoveshchenskaya, N. F., Borisova, T. D., Egorov, I. M., Zagorskiy, G. A., & Kovalev, A. S. (2023). Features of narrowband stimulated electromagnetic emission depending on the effective radiated power of the EISCAT/Heating facility. *Cosmic Research*, *61*(6), 501–509. https://doi.org/10.1134/s0010952523700478

Kastinen, D., Vierinen, J., Grydeland, T., & Kero, J. (2023). Using radar beam-parks to characterize the Kosmos-1408 fragmentation event. *Acta Astronautica*, *202*, 341–359. https://doi.org/10.1016/j.actaastro.2022.10.021

Kauristie, K., Marghitu, O., van de Kamp, M., Hoppe, T., Honkonen, I., Blagau, A., Ivan, I. M., Codrescu, M., Ridley, A., Tóth, G., Ogawa, Y., & Trenchi, L. (2024). Joule heating rate at high-latitudes by Swarm and ground-based observations compared to MHD simulations. *Journal of Atmospheric and Solar-Terrestrial Physics*, *260*, 106254. https://doi.org/10.1016/j.jastp.2024.106254

Kim, E., Jee, G., Wang, W., Kwak, Y.-S., Shim, J.-S., Ham, Y.-B., & Kim, Y. H. (2023). Hemispheric asymmetry of the polar ionospheric density investigated by ESR and JVD radar observations and TIEGCM simulations for the Solar minimum period. *Journal of Geophysical Research: Space Physics*, *128*(2), e2022JA031126. https://doi.org/10.1029/2022ja031126

Krasheninnikov, I. V., & Shubin, V. N. (2024). Influence of large-scale auroral inhomogeneities on the passage of radio waves under moderate geomagnetic storm conditions. *Geomagnetism and Aeronomy*, *64*(5), 663–672. https://doi.org/10.1134/s0016793224600607

Kvammen, A., Vierinen, J., Huyghebaert, D., Rexer, T., Spicher, A., Gustavsson, B., & Floberg, J. (2024). NOIRE-Net–a convolutional neural network for automatic classification and scaling of high-latitude ionograms. *Frontiers in Astronomy and Space Sciences*, *11*, 1289840. https://doi.org/10.3389/fspas.2024.1289840

Lanchester, B. (2023). In praise of the unexpected. *Perspectives of Earth and Space Scientists*, *4*(1), e2023CN000209. https://doi.org/10.1029/2023cn000209

Lessard, M. R., Damsell, A., Sadler, F. B., Oksavik, K., & Clausen, L. (2023). Interhemispheric asymmetries of neutral upwelling and ion upflow. *Frontiers in Astronomy and Space Sciences*, *10*(1151016). https://doi.org/10.3389/fspas.2023.1151016

Leyser, T. B., Sergienko, T., Brändström, U., Gustavsson, B., & Rietveld, M. T. (2023). On mechanisms for high-frequency pump-enhanced optical emissions at 557.7 and 630.0 nm from atomic oxygen in the high-latitude F-region ionosphere. *Annales Geophysicae*, *41*(2), 589–600. https://doi.org/10.5194/angeo-41-589-2023

Li, Y., Li, H., Wu, J., Lyu, X., Chai, Y., Yuan, C., & Zhou, Z. (2024). Artificial excitation and propagation of ultra-low frequency signals in the polar ionosphere. *Physics of Plasmas*, *31*(8), 082901. https://doi.org/10.1063/5.0202317

Li, Y., Li, H., Wu, J., Lyu, X., Yuan, C., Li, C., & Zhou, Z. (2023). Effect of wave polarization on ionospheric Ohmic heating and optimal polarization. *Physics of Plasmas*, *30*(10), 102902. https://doi.org/10.1063/5.0158960

Lukianova, R. Y. (2023). The influence of field-aligned currents on electron density in the ionosphere: Combined observations of SWARM satellites and ESR radar. *Cosmic Research*, *61*(6), 491–500. https://doi.org/10.1134/s0010952523700454

Ma, L., Yu, Y., Tong, X., Tang, L., Liu, W., Cao, J., Wu, J., & Wu, J. (2024). Quasi-periodic EMIC waves and pulsating ionospheric perturbations related to ULF waves. *Journal of Geophysical Research: Space Physics*, *129*(9), e2024JA032657. https://doi.org/10.1029/2024ja032657

Ma, Y.-Z., Zhang, Q.-H., Lyons, L., Oksavik, K., Xing, Z.-Y., Hairston, M., Nanan, B., Hu, Z.-J., Wang, Y., & Zhao, S.-H. (2023). A comparative study on the hot dense plasma and cold patch by using multi-instrument observations. *Journal of Geophysical Research: Space Physics*, *128*(6), e2022JA031166. https://doi.org/10.1029/2022ja031166

Madhanakumar, M., Spicher, A., Vierinen, J., & Oksavik, K. (2024). On the strength of E and F region irregularities for GNSS scintillation in the dayside polar ionosphere. *Journal of Atmospheric and Solar-Terrestrial Physics*, *256*, 106197. https://doi.org/10.1016/j.jastp.2024.106197

Madhanakumar, M., Spicher, A., Vierinen, J., Oksavik, K., Coster, A. J., Huyghebaert, D. R., Martin, C. J., Häggström, I., & Paxton, L. J. (2024). The growth and decay of intense GNSS amplitude and phase scintillation during non-storm conditions. *Space Weather*, *22*(12), e2024SW004108. https://doi.org/10.1029/2024sw004108

Matuura, N., Fujii, R., & Nozawa, S. (2023). History of EISCAT – Part 6: The participation of Japan in the EISCAT Scientific Association. *History of Geo- and Space Sciences*, *14*(1), 61–69. https://doi.org/10.5194/hgss-14-61-2023

Murase, K., Kataoka, R., Nishiyama, T., Sato, K., Tsutsumi, M., Tanaka, Y., Ogawa, Y., & Sato, T. (2023). Atmospheric ionizations by Solar X-rays, Solar protons, and radiation belt electrons in September 2017 space weather event. *Space Weather*, *21*(12), e2023SW003651. https://doi.org/10.1029/2023sw003651

Nishiyama, T., Kagitani, M., Furutachi, S., Iwasa, Y., Ogawa, Y., Tsuda, T. T., Dalin, P., Tsuchiya, F., Nozawa, S., & Sigernes, F. (2024). The first simultaneous spectroscopic and monochromatic imaging observations of short-wavelength infrared aurora of N_2^+ Meinel (0,0) band at 1.1 μm with incoherent scatter radar. *Earth, Planets and Space*, *76*(1), 30. https://doi.org/10.1186/s40623-024-01969-x

Norberg, J., Käki, S., Roininen, L., Mielich, J., & Virtanen, I. I. (2023). Model-free approach for regional ionospheric multi-instrument imaging. *Journal of Geophysical Research: Space Physics*, *128*(1), e2022JA030794. https://doi.org/10.1029/2022ja030794

Nykiel, G., Ferreira, A., Günzkofer, F., Iochem, P., Tasnim, S., & Sato, H. (2024). Large-scale traveling ionospheric disturbances over the European sector during the geomagnetic storm on March 23-24, 2023: Energy deposition in the source regions and the propagation characteristics. *Journal of Geophysical Research: Space Physics*, *129*(3), e2023JA032145. https://doi.org/10.1029/2023ja032145

Oyama, S., Hosokawa, K., Vanhamäki, H., Aikio, A., Sakanoi, T., Cai, L., Virtanen, I. I., Shiokawa, K., Nishitani, N., Shinbori, A., & Ogawa, Y. (2023). IMF dependence of midnight bifurcation in the thermospheric wind at an auroral latitude based on nine winter measurements in Tromsø, Norway. *Geophysical Research Letters*, *50*(14), e2023GL104334. https://doi.org/10.1029/2023gl104334

Oyama, S., Vanhamäki, H., Cai, L., Shinbori, A., Hosokawa, K., Sakanoi, T., Shiokawa, K., Aikio, A., Virtanen, I. I., Ogawa, Y., Miyoshi, Y., Kurita, S., & Nishitani, N. (2024). Thermospheric wind response to March 2023 storm: Largest wind ever observed with a Fabry-Perot interferometer in Tromsø, Norway since 2009. *Space Weather*, *22*(3), e2023SW003728. https://doi.org/10.1029/2023sw003728

Pellinen-Wannberg, A. (2023). Even a blind chicken sometimes finds a grain of corn — In my case in space. *Perspectives of Earth and Space Scientists*, *4*(1), e2022CN000176. https://doi.org/10.1029/2022cn000176

Rauf, A., Li, H. L., Ullah, S., Meng, L., Wang, B., Ge, S. C., & Wang, M. (2023). Effects of energetic particle precipitation on electron temperature in the E-region of ionosphere: An experimental study. *Geomagnetism and Aeronomy*, *63*(1), 30–40. https://doi.org/10.1134/s0016793222600758

Reistad, J. P., Hatch, S. M., Laundal, K. M., Oksavik, K., Zettergren, M., Vanhamäki, H., & Virtanen, I. (2024). Volumetric reconstruction of ionospheric electric currents from tri-static incoherent scatter radar measurements. *Journal of Geophysical Research: Space Physics*, *129*(8), e2024JA032744. https://doi.org/10.1029/2024ja032744

Rietveld, M., & Senior, A. (2023). Comment on Blagoveshchenskaya et al. Artificial ducts created via high-power HF radio waves at EISCAT. Remote Sens. 2023, 15, 2300. *Remote Sensing*, *15*(17), 4294. https://doi.org/10.3390/rs15174294

Robert, E., Barthelemy, M., Cessateur, G., Woelfflé, A., Lamy, H., Bouriat, S., Gullikstad Johnsen, M., Brändström, U., & Biree, L. (2023). Reconstruction of electron precipitation spectra at the top of the upper atmosphere using 427.8 nm auroral images. *Journal of Space Weather and Space Climate*, *13*, 30. https://doi.org/10.1051/swsc/2023028

Schreiter, L., Stolle, C., Rauberg, J., Kervalishvili, G., van den Ijssel, J., Arnold, D., Xiong, C., & Callegare, A. (2023). Topside ionosphere sounding from the CHAMP, GRACE, and GRACE-FO missions. *Radio Science*, *58*(3), e2022RS007552. https://doi.org/10.1029/2022rs007552

Sergeev, V. A., Stepanov, N. A., Ogawa, Y., Rozanov, E. V., & Shukhtina, M. A. (2024). Local time distribution and activity dependence of extreme electron densities in the auroral D-region as an image of energy-dependent energetic electron precipitation. *Journal of Geophysical Research: Space Physics*, *129*(10), e2024JA032913. https://doi.org/10.1029/2024ja032913

Sergienko, T., Yokoyama, Y., Brändström, U., Yamauchi, M., & Tjulin, A. (2024). Ionospheric fireworks illuminate auroral science. *Eos*, *105*, . https://doi.org/10.1029/2024eo240083

Stamm, J., Vierinen, J., Gustavsson, B., & Spicher, A. (2023). A technique for volumetric incoherent scatter radar analysis. *Annales Geophysicae*, *41*(1), 55–67. https://doi.org/10.5194/angeo-41-55-2023

Stober, G., Weryk, R., Janches, D., Dawkins, E. C., Günzkofer, F., Hormaechea, J. L., & Pokhotelov, D. (2023). Polarization dependency of transverse scattering and collisional coupling to the ambient atmosphere from meteor trails — theory and observations. *Planetary and Space Science*, *237*, 105768. https://doi.org/10.1016/j.pss.2023.105768

Swarnalingam, N., Wu, D. L., Emmons, D. J., & Gardiner-Garden, R. (2023). Optimal estimation inversion of ionospheric electron density from GNSS-POD limb measurements: Part II-Validation and comparison using NmF2 and hmF2. *Remote Sensing*, *15*(16), 4048. https://doi.org/10.3390/rs15164048

Tanaka, Y., Ogawa, Y., Kadokura, A., Aso, T., Gustavsson, B., Brändström, U., Sergienko, T., Ueno, G., & Saita, S. (2024). Application of generalized aurora computed tomography to the EISCAT_3D project. *Annales Geophysicae*, *42*(1), 179–190. https://doi.org/10.5194/angeo-42-179-2024

Tariku, Y. A. (2024). The geomagnetic storm time responses of the TEC, foF2, and hmF2 in different Solar activity during Solar cycle 24 and 25. *Radio Science*, *59*(12), e2024RS007961. https://doi.org/10.1029/2024rs007961

Tesfaw, H. W., Virtanen, I. I., & Aikio, A. T. (2023). Characteristics of auroral electron precipitation at geomagnetic latitude 67° over Tromsø. *Journal of Geophysical Research: Space Physics*, *128*(7), e2023JA031382. https://doi.org/10.1029/2023ja031382

Themens, D. R., Elvidge, S., McCaffrey, A., Jayachandran, P. T., Coster, A., Varney, R. H., Galkin, I., Goodwin, L. V., Watson, C., Maguire, S., Kavanagh, A. J., Zhang, S.-R., Goncharenko, L., Bhatt, A., Dorrian, G., Groves, K., Wood, A. G., & Reid, B. (2024). The high latitude ionospheric response to the major May 2024 geomagnetic storm: A synoptic view. *Geophysical Research Letters*, *51*(19), e2024GL111677. https://doi.org/10.1029/2024gl111677

Thorell, A. (2023). *Sporadic-E layers in the polar cap ionosphere: A review on Es occurrence, dynamics and formation theory* [MSc Thesis]. KTH Royal Institute of Technology, Sweden. https://urn.kb.se/resolve?urn=urn:nbn:se:kth:diva-343532

Ullah, S., Li, H., Rauf, A., Khan, S. U., Khan, S. U., Ge, S., Wang, B., Wang, M., & Meng, L. (2023). A comparative study of heating effects on PMSE between the naturally occurred mono double and tri layers. *Geomagnetism and Aeronomy*, *63*(1), 51–67. https://doi.org/10.1134/s0016793222600540

Ullah, S., Li, H., Rauf, A., Ullah Khan, S., Ullah Khan, S., Ge, S., Wang, B., Wang, M., & Meng, L. (2023). Comparison of the reaction of polar mesosphere winter echoes and polar mesosphere summer echoes to high-frequency heating in terms of modulated characteristics. *Earth and Planetary Physics*, *7*(2), 247–256. https://doi.org/10.26464/epp2023029

van Hazendonk, C. M., Baddeley, L., Laundal, K. M., & Chau, J. L. (2024). Detection and energy dissipation of ULF waves in the polar ionosphere: A case study using the EISCAT radar. *Journal of Geophysical Research: Space Physics*, *129*(7), e2024JA032633. https://doi.org/10.1029/2024ja032633

Virtanen, I. I., Tesfaw, H. W., Aikio, A. T., Varney, R., Kero, A., & Thomas, N. (2024). F1 region ion composition in Svalbard during the International Polar Year 2007–2008. *Journal of Geophysical Research: Space Physics*, *129*(3), e2023JA032202. https://doi.org/10.1029/2023ja032202

Walach, M.-T., Soobiah, Y., Carter, J. A., Whiter, D. K., Kavanagh, A. J., Hartinger, M. D., Oksavik, K., Salzano, M. L., & Archer, M. O. (2024). SMILE winter campaign. *RAS Techniques and Instruments*, *3*(1), 556–564. https://doi.org/10.1093/rasti/rzae038

Wang, X., Cai, L., Aikio, A., Vanhamäki, H., Virtanen, I., Zhang, Y., Luo, B., & Liu, S. (2024). Ionospheric conductances due to electron and ion precipitations: A comparison between EISCAT and DMSP estimates. *Journal of Geophysical Research: Space Physics*, *129*(2), e2023JA032354. https://doi.org/10.1029/2023ja032354

Wu, J., Wu, J., Feng, J., Li, Q., Hao, S., Xu, Z., Zhao, H., & Zhang, Y. (2024). The nature of electron density enhancement over a wide altitude range during ionosphere heating experiments at EISCAT. *Earth and Planetary Physics*, *8*(2), 1–7. https://doi.org/10.26464/epp2024005

Xiong, Y.-T., Han, D.-S., Wang, Z.-w., Shi, R., & Feng, H.-T. (2024). Intermittent lobe reconnection under prolonged northward interplanetary magnetic field condition: Insights from cusp spot event observations. *Geophysical Research Letters*, *51*(2), e2023GL106387. https://doi.org/10.1029/2023gl106387

Zhang, D., Zhang, Q.-H., Oksavik, K., Xu, T., Xing, Z.-Y., Lyons, L. R., Han, D.-S., Zhang, H.-B., Ma, Y.-Z., Hu, Z.-J., Liu, J.-J., Wang, Y., & Wang, X.-Y. (2023). Do the throat auroras create polar cap patches? *Geophysical Research Letters*, *50*(7), e2022GL102263. https://doi.org/10.1029/2022gl102263

Zhang, J., Sun, T., Yu, X., Li, D., Li, H., Guo, J., Ding, Z., Chen, T., Wu, J., & Wang, C. (2024). Analysis of the joint detection capability of the SMILE satellite and EISCAT-3D radar. *Earth and Planetary Physics*, *8*(1), 299–306. https://doi.org/10.26464/epp2023061

Zhou, Q., Li, Y., & Gong, Y. (2024). A multivariable study of a traveling ionosphere disturbance using the Arecibo incoherent scatter radar. *Remote Sensing*, *16*(21), 4104. https://doi.org/10.3390/rs16214104

Žigman, V., Dominique, M., Grubor, D., Rodger, C. J., & Clilverd, M. A. (2023). Lower-ionosphere electron density and effective recombination coefficients from multi-instrument space observations and ground VLF measurements during solar flares. *Journal of Atmospheric and Solar-Terrestrial Physics*, *247*, 106074. https://doi.org/10.1016/j.jastp.2023.106074

EISCAT Operations 2023–2024

EISCAT Scientific Association operates three radar systems (UHF, VHF and ESR) with transmitters on two geographical locations, working in three different radio frequency ranges.

The UHF (Ultra High Frequency) system operates at a frequency range around 929 MHz with a transmitter and receiver on the Ramfjordmoen site near Tromsø. The antenna is a 32 m steerable parabolic dish. The lowest elevation that is allowed to be used for radio transmissions from the UHF antenna is 25°.

The VHF (Very High Frequency) system operates at a frequency range around 224 MHz with a transmitter and receiver on the same site as the UHF system (Ramfjordmoen near Tromsø). The antenna consists of four 30 m × 40 m tiltable rectangular dishes. The VHF antenna is allowed to be used for radio transmissions from the zenith direction, and northward down to 25°, No transmissions are allowed in any southward direction.

The ESR (EISCAT Svalbard Radar) system operates at a frequency range around 500 MHz with a transmitter and receiver at Longyearbyen on Svalbard. The system consists of two antennas: one fully steerable 32 m parabolic dish, and one fixed 42 m parabolic dish pointing in the direction of the local magnetic field. This set-up enables simultaneous measurements in two different directions.

The EISCAT radar systems operate in two basic modes, using approximately half the available observing time for each. In the Special Programme (SP) mode, users from EISCAT members countries conduct individual campaigns dedicated to specific research objectives, with the resulting data reserved for that user for some time. Common Programmes are conducted by EISCAT for the benefit of the entire user community and the resulting data are immediately available to all EISCAT members.

The UHF and VHF radars can be operated simultaneously during the Common Programme experiments. Such observations offer comprehensive data sets for atmospheric, ionospheric, and magnetospheric studies.

Common Programme One, CP-1
Common Programme One, CP-1, uses a fixed transmitting antenna, pointing along the geomagnetic field direction. CP-1 is capable of providing results with very good time resolution and is suitable for the study of substorm phenomena, particularly auroral processes where conditions might change rapidly. On longer time scales, CP-1 measurements support studies of diurnal changes, such as atmospheric tides, as well as seasonal and solar-cycle variations.

Common Programme Two, CP-2
Common Programme Two, CP-2 does small antenna scan. The scan uses three positions, vertical, field-aligned and west (east), and a full scan takes 4 min. One aim of the scan is to identify wave-like phenomena with length and time scales comparable with, or larger than, the scan (a few tens of kilometers and about ten minutes).

Common Programme Three, CP-3
Common Programme Three, CP-3, covers a 10° latitudinal range in the F-region with a 16-position scan up to 74°N in a 24 min cycle. The observations are made in a plane defined by the magnetic meridian through Tromsø.ition scan that takes 24 min. The main aim of CP-3 is the mapping of ionospheric and electrodynamic parameters over a broad latitude range.

Common Programme Four, CP-4
Common Programme Four, CP-4, covers geographic latitudes up to almost 80°N (77°N invariant latitude) using a low elevation, with a possible split-beam configuration. CP-4 is particularly suitable for studies of high latitude plasma convection and polar cap phenomena. However, with the present one-beam configuration of the VHF radar, CP-4 is run with either simultaneous UHF and VHF radars, or with UHF only in a two position scan taking 4 min.

Common Programme Six, CP-6
Common Programme Six, CP-6, is designed for low altitude studies, providing spectral measurements at mesospheric heights. Velocity and electron density are derived from the measurements and the spectra contain information on the aeronomy of the mesosphere. Vertical antenna pointing is used.

Common Programme Seven, CP-7
Common Programme Seven, CP-7, probes high altitudes and is particularly aimed at polar wind studies. The present version, with only one of the VHF klystrons running, is designed to cover altitudes up to 1500 km vertically above Ramfjordmoen.

Equivalent Common Programme modes are available for the EISCAT Svalbard Radar.

Common Programme One, CP-1
CP-1 is directed along the local geomagnetic field (81.6° inclination).

Common Programme Two, CP-2
CP-2 uses a two position scan with the 32 m antenna, with the 42 m antenna measuring while the 32 m antenna is moving. The full scan takes 3 min.

Common Programme Three, CP-3
CP-3 is a 14 position elevation scan with south beam swinging positions of the 32 m antenna, with the 42 m antenna measuring during the motion. The full scan takes 24 min.

Common Programme Four, CP-4
CP-4 combines observations in the F-region (42 m antenna) with a two low-elevation direction scan (32 m antenna), which can be either northward or southward. The full scan takes 4 min.

Common Programme Six, CP-6
CP-6 is similar to the mainland radar CP-6.

Common Programme Seven, CP-7
CP-7 is similar to the mainland radar CP-7.

The tables on the next four pages summarise the accounted hours on the various facilities for each month and for each Common Programme mode (CP) or Associate (SP) for the years 2023 and 2024.

KST COMMON PROGRAMMES

2023	Jan	Feb	Mar	Apr	May	Jun	Jul	Aug	Sept	Oct	Nov	Dec	Total	%	Target%
CP1	1.5	37.5	81						43		14	14	191	43	16
CP2	61	106											167	37	16
CP3													0	0	12
CP4								3					3	1	10
CP6		17.5			4.5	62.5							84.5	19	20
CP7								3					3	1	18
UP													0	0	
Total	62.5	161	81	0	4.5	62.5	0	6	43	0	14	14	**448.5**	100	
%	14	36	18	0	1	14	0	1	10	0	3	3	100		

KST SPECIAL PROGRAMMES

2023	Jan	Feb	Mar	Apr	May	Jun	Jul	Aug	Sept	Oct	Nov	Dec	Total	Incl AA	Move	Target
CN									15				15	17		35
FI		6	43									52.5	101.5	108		126
NI		9	37.5						11			16	73.5	78		86
NO	1.5	0.5	56.5				2	24	18		42	94.5	239	256		352
SW		5.5	52.5	14	17		2	28	14	18			151	163		247
UK	24		30		16	22			5.5				97.5	104		133
AA									8	20	12	8	48			
Total	25.5	21	219.5	14	33	22	4	52	71.5	38	54	171	**725.5**	**726**	**0**	**973**
%	4	3	30	2	5	3	1	7	10	5	7	24	100			

	EI	CN	FI	NI	NO	SW	UK	
Target		3.64	12.92	8.83	36.21	25.38	13.7	%

KST OTHER PROGRAMMES

2023	Jan	Feb	Mar	Apr	May	Jun	Jul	Aug	Sept	Oct	Nov	Dec	Total	Target
PP			16									42	58	58
EI													0	28
GE			5.5							10.5	19.5		35.5	27
FR													0	0
UA													0	5
KR													0	56
US												0.5	0.5	8
TB													0	0
Total	0	0	21.5	0	0	0	0	0	0	10.5	19.5	42.5	**94**	**182**

KST TOTALS

2023	Jan	Feb	Mar	Apr	May	Jun	Jul	Aug	Sept	Oct	Nov	Dec	Total	Target
CP	62.5	161	81	0	4.5	62.5	0	6	43	0	14	14	448.5	450
SP	25.5	21	219.5	14	33	22	4	52	71.5	38	54	171	725.5	973
OP	0	0	21.5	0	0	0	0	0	0	10.5	19.5	42.5	94	182
Total	88	182	322	14	37.5	84.5	4	58	114.5	48.5	87.5	227.5	**1268**	**1605**

USAGE BREAKDOWN

2023	Jan	Feb	Mar	Apr	May	Jun	Jul	Aug	Sept	Oct	Nov	Dec	Total	Target
UHF	75.5	161.5	289.5	14	25	9			97.5	36.5	57	166.5	932	705
VHF	12	17.5	30		12.5	75.5	4	58	17.5		0.5	60	287.5	705
ESR	144	162.5	246.5	9	0	37	0	0	7.5	1	48.5	29	685	805
Heating	0.5	2.5	2.5							12.5	29	0.5	47.5	135
Total Radar	232	344	568.5	23	37.5	121.5	4	58	122.5	50	135	256	1952.5	2350
Passive KST											4		4	300
Passive ESR													0	

ESR COMMON PROGRAMMES

2023	Jan	Feb	Mar	Apr	May	Jun	Jul	Aug	Sept	Oct	Nov	Dec	Total	%	Target%
CP1	63	149.5	163.5	2					2	1	43.5	22	446.5	93	54
CP2													0	0	16
CP3													0	0	12
CP4													0	0	10
CP6			2			32							34	7	
CP7													0	0	
UP													0	0	
Total	63	149.5	165.5	2	0	32	0	0	2	1	43.5	22	**480.5**	100	
%	13	31	34	0	0	7	0	0	0	0	9	5	100		

ESR SPECIAL PROGRAMMES

2023	Jan	Feb	Mar	Apr	May	Jun	Jul	Aug	Sept	Oct	Nov	Dec	Total	Incl AA	Move	Target
CN													0	0	0	12
FI			36									7	43	43	0	43
NI	14		15										29	29	0	29
NO		5	16						1.5		5		27.5	28	0	121
SW			14	7		5			4				30	30	0	85
UK	67	8											75	75	0	46
AA													0			
Total	81	13	81	7	0	5	0	0	5.5	0	5	7	**204.5**	**205**	**0**	**333**
%	40	6	40	3	0	2	0	0	3	0	2	3	100			

ESR OTHER PROGRAMMES

2023	Jan	Feb	Mar	Apr	May	Jun	Jul	Aug	Sept	Oct	Nov	Dec	Total	Target
PP													0	0
EI													0	22
GE													0	0
FR													0	0
UA													0	0
KR													0	0
TB													0	0
Total	0	0	0	0	0	0	0	0	0	0	0	0	**0**	**22**

ESR TOTALS

2023	Jan	Feb	Mar	Apr	May	Jun	Jul	Aug	Sept	Oct	Nov	Dec	Total	Target
CP	63	149.5	165.5	2	0	32	0	0	2	1	43.5	22	480.5	450
SP	81	13	81	7	0	5	0	0	5.5	0	5	7	204.5	333
OP	0	0	0	0	0	0	0	0	0	0	0	0	0	22
Total	144	162.5	246.5	9	0	37	0	0	7.5	1	48.5	29	**685**	**805**

KST COMMON PROGRAMMES

2024	Jan	Feb	Mar	Apr	May	Jun	Jul	Aug	Sept	Oct	Nov	Dec	Total	%	Target%
CP1		124							128.5	31.5	1.5		285.5	81	16
CP2													0	0	16
CP3													0	0	12
CP4								3					3	1	10
CP6								3.5	30.5	29		2	65	18	20
CP7													0	0	18
UP													0	0	
Total	0	124	0	0	0	0	0	6.5	159	60.5	1.5	2	**353.5**	100	
%	0	35	0	0	0	0	0	2	45	17	0	1	100		

KST SPECIAL PROGRAMMES

2024	Jan	Feb	Mar	Apr	May	Jun	Jul	Aug	Sept	Oct	Nov	Dec	Total	Incl AA	Move	Target
CN											15		15	18		29
FI			24.5					24			15	40	103.5	116		135
NI			46.5								4	20	70.5	76		62
NO			27	12			72			12	19.5	56	198.5	230		325
SW		50	54		16	38.5		46.5			4		209	228		199
UK	48			10	20		27.5	12	4	20	0		141.5	152		108
AA	14	16								16.5	22.5	13	82			
Total	62	66	152	22	36	38.5	99.5	82.5	4	48.5	80	129	**820**	**820**	**0**	**858**
%	8	8	19	3	4	5	12	10	0	6	10	16	100			

	EI	CN	FI	NI	NO	SW	UK	
Target		3.39	15.75	7.28	37.87	23.14	12.57	%

KST OTHER PROGRAMMES

2024	Jan	Feb	Mar	Apr	May	Jun	Jul	Aug	Sept	Oct	Nov	Dec	Total	Target
PP										10	12.5	11	33.5	112
TNA								5	8				13	
EI						1							1	28
DLR			6								14		20	31
UKSA						8					24		32	70
UA													0	0
KR											47		47	0
NEURA						9							9	
METI	4												0	8
TB													0	0
Total	4	0	6	0	0	18	0	5	8	10	97.5	11	**155.5**	**249**

KST TOTALS

2024	Jan	Feb	Mar	Apr	May	Jun	Jul	Aug	Sept	Oct	Nov	Dec	Total	Target
CP	0	124	0	0	0	0	0	6.5	159	60.5	1.5	2	353.5	522
SP	62	66	152	22	36	38.5	99.5	82.5	4	48.5	80	129	820	858
OP	4	0	6	0	0	18	0	5	8	10	97.5	11	159.5	249
Total	66	190	158	22	36	56.5	99.5	94	171	119	179	142	**1333**	**1629**

USAGE BREAKDOWN

2024	Jan	Feb	Mar	Apr	May	Jun	Jul	Aug	Sept	Oct	Nov	Dec	Total	Target
UHF	42	162	106.5	17	18	35	36	28	167	72	168.5	77.5	929.5	750
VHF	24.5	0	24	5	18	22	64	63.5	4	46.5	10.5	64.5	346.5	750
ESR	42.5	166	13	1.5	112	11	0	35.5	146	0	0	0	527.5	984
Heating		28	28					2					58	129
Total Radar	109	356	171.5	23.5	148	68	100	129	317	118.5	179	142	1861.5	2613
Passive KST													0	0
Passive ESR													0	

ESR COMMON PROGRAMMES

2024	Jan	Feb	Mar	Apr	May	Jun	Jul	Aug	Sept	Oct	Nov	Dec	Total	%	Target%
CP1		147.5	2	1.5	96	3		6	146				402	100	0
CP2													0	0	0
CP3													0	0	0
CP4													0	0	0
CP6													0	0	
CP7													0	0	
UP													0	0	
Total	0	147.5	2	1.5	96	3	0	6	146	0	0	0	**402**	100	
%	0	37	0	0	24	1	0	1	36	0	0	0	100		

ESR SPECIAL PROGRAMMES

2024	Jan	Feb	Mar	Apr	May	Jun	Jul	Aug	Sept	Oct	Nov	Dec	Total	Incl AA	Move	Target
CN													0	0	0	14
FI													0	0	0	67
NI			7										7	7	0	31
NO		18.5	4					2					24.5	25	0	161
SW					8	8							16	16	0	98
UK	24							4					28	28	0	53
AA													0			
Total	24	18.5	11	0	8	8	0	6	0	0	0	0	**75.5**	**76**	**0**	**424**
%	32	25	15	0	11	11	0	8	0	0	0	0	100			

ESR OTHER PROGRAMMES

2024	Jan	Feb	Mar	Apr	May	Jun	Jul	Aug	Sept	Oct	Nov	Dec	Total	Target
PP	18.5							23.5					42	88
TNA					8								8	
EI													0	22
DLR													0	0
UKSA													0	0
UA													0	0
KR													0	54
TB													0	0
Total	18.5	0	0	0	8	0	0	23.5	0	0	0	0	**50**	**164**

ESR TOTALS

2024	Jan	Feb	Mar	Apr	May	Jun	Jul	Aug	Sept	Oct	Nov	Dec	Total	Target
CP	0	147.5	2	1.5	96	3	0	6	146	0	0	0	402	396
SP	24	18.5	11	0	8	8	0	6	0	0	0	0	75.5	424
OP	18.5	0	0	0	8	0	0	23.5	0	0	0	0	50	164
Total	42.5	166	13	1.5	112	11	0	35.5	146	0	0	0	**527.5**	**984**

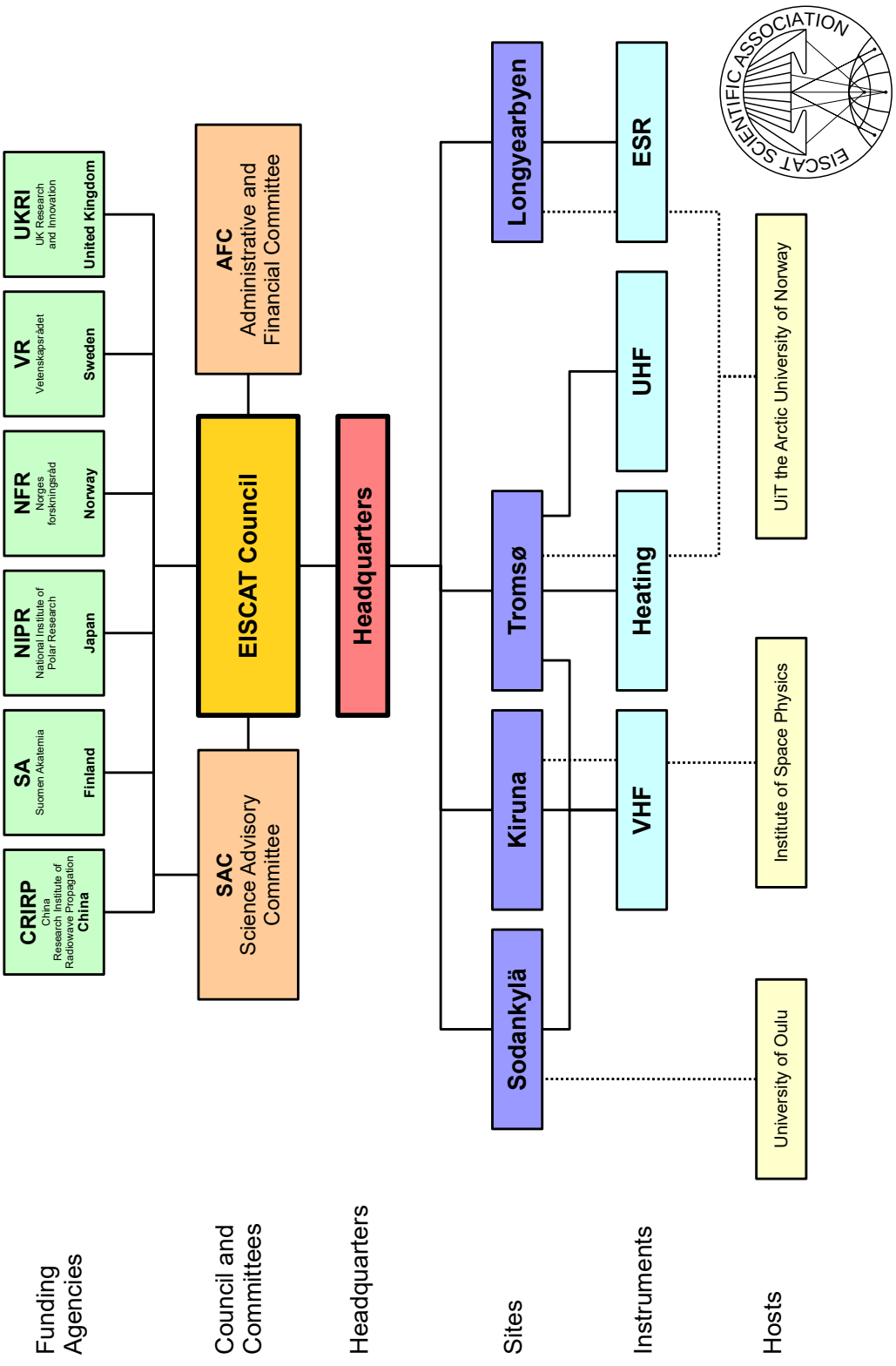

EISCAT organisational diagram, December 2024.

Photo from the Annual Review Meeting, 18–19 October 2023, at Cape East in Haparanda, Sweden. From left: Axel Steuwer, Carl-Fredrik Enell, Robert Juhlin, Mária Mihálíková, Tutti Johansson Falk, Stian Grande, Juri Katkalov, Anders Tjulin, Henrik Andersson, Elisabet Goth, Magnus Thorebäck, Espen Helgesen, Thomas Ulich, Simon Brown, Emma Unander, Arild Stenberg, Trond Sandmo, Erik Varberg, Jussi Markkanen, Assar Westman, David Rutberg, Harri Hellgren, Johan Svensson.

EISCAT Scientific Association

November 2024

EISCAT Director

Dr. A. Steuwer

EISCAT Council

P. R. of China	
Prof. X. Chen	Delegate
Dr. Z. Ding	
Prof. J. Wu	
Finland	
Prof. A. Aikio	
Dr. K. Sulonen	Delegate
Prof. P. Verronen	
Japan	
Prof. H. Miyaoka	Delegate
Dr. S. Nozawa	
Norway	
Prof. P. Espy	
Prof. I. Mann	
Dr. P. Sørgaard	Delegate
Sweden	
Dr. T. Andersson	
Prof. J. Gumbel	*Chair*
Dr. O. Norberg	
Dr. M. Thuveson	Delegate
United Kingdom	
Prof. M. Freeman	Delegate
Prof. I. W. McCrea	

Administrative and Finance Committee (AFC)

Dr. R. Chaplin	*Chair*, United Kingdom
Dr. M. Friberg	Sweden
Prof. H. Miyaoka	Japan
Dr. I. Solheim	Norway
Ms. M. Vannas	Finland

Scientific Advisory Committee (SAC)

Dr. S. Buchert	Sweden
Prof. L. Clausen	*Chair*, Norway
Dr. K. Hosokawa	Japan
Dr. A. Kavanagh	United Kingdom
Dr. A. Kero	Finland
Dr. A. Strømme	External member
Prof. J. Wu	P. R. of China
Representatives	Affiliates

Senior Management

Mr. H. Andersson	Head of Adm., Deputy Dir.
Dr. A. Steuwer	Director

Site Leaders

Mr. E. Helgesen	EISCAT Svalbard Radar
Mr. A. Stenberg	Tromsø Site

Appendix:

EISCAT Scientific Association Annual Report, 2023

EISCAT Scientific Association
Registered as a Swedish non-profit organisation
Organisation number: 897300-2549

Annual financial report for the year 2023-01-01 – 2023-12-31

The EISCAT Council and the Director for the Association submits herewith the annual report for 2023.

Content	**Page**
Administration report	2
Profit and loss accounts	5
Balance sheet	6
Statement of cash flows	7
Notes	8

ADMINISTRATION REPORT

Ownership, organisation and objective
The EISCAT Scientific Association was established in 1975 through an agreement between six European organisations. Japan joined in 1996 and the People's Republic of China in 2007.

The EISCAT Associates at 2023-12-31 are: China Research Institute of Radiowave Propagation (People's Republic of China), National Institute of Polar Research (Japan), Norges forskningsråd (Norway), Suomen Akatemia (Finland), UK Research and Innovation (United Kingdom of Great Britain and Northern Ireland) and Vetenskapsrådet (Sweden).

The now-running EISCAT Agreement came into force 2017-06-20, with all Associates making long term funding commitments to the Association. The Association has its formal seat in Kiruna, Sweden, and is registered as a non-profit organisation.

The aim of the Association is to make significant progress in the understanding of physical processes in geospace, in the high latitude atmosphere, and in the coupling between the high and low latitudes and altitudes. For this purpose, the Association has developed, constructed, and now operates, a number of radar facilities at high latitudes. At present, these comprise a system of stations at Tromsø (Norway), Kiruna (Sweden), Sodankylä (Finland), and Longyearbyen (Svalbard). The new system, EISCAT_3D, is currently being constructed.

The Association is fully funded by the Associates, but additional operations may also be funded by short term additional contributions from both Associate and non-Associate bodies. Depending on the available funding, scientific priorities and operational targets are adjusted on an annual basis.

The EISCAT Council is charged with the overall administration and supervision of the Association's activities. The Council appoints a Director, who is responsible for the daily management and operation of the facilities of the Association.

Operation and scientific development
The EISCAT Radars systems operated reliably throughout the year and 1 957 hours were accounted in 2023 (2 007 hours in 2022).

Common Programmes amounted to 47.5% (38%) of the operations. Special Programmes amounted to 47.5% (52%) and other operations amounted to 5% (10%) of the total hours.

The German Affiliate made use of their access to the systems and totally 58 hours (140 hours) were accounted the affiliates. The Peer-Review Programme (PP) made it possible for user groups from Finland and USA to run experiments, at no cost, on the systems. PP-time amounted to 40 accounted hours (36 hours). The Transnational Access (TNA) project, PITHIA-NRF, did not fund any campaigns in 2023. Totally 0 hours (18 hours) were TNA-hours.

Future operation and scientific development
The current EISCAT systems are ready for users. These include the EISCAT Svalbard Radar, Heating and the UHF and VHF radars. Due to system failures, the tristatic VHF mode had to be cancelled in 2023. The two VHF receive sites in Finland and Sweden will be decommissioned in 2024. Tristatic, or rather multistatic, operations will again be possible when the new EISCAT_3D system is taken in use.

The EISCAT_3D radar system is soon to be completed. It will replace the current UHF and VHF radar systems. We plan for a first-light measurement mid-2024 and full operations in 2025.

The old mainland UHF and VHF radar systems, which will be replaced by the new EISCAT_3D system, will be decommissioned soon after the new system is operational.

Project activities
In 2023, two of the externally EU-funded projects came to a close; EGI-ACE and ENVRI-FAIR. PITHIA-NRF continues into 2025. Two new EU-funded projects start in 2024, ARC-TREE and INPROCAP. The EISCAT involvement in the two new projects are very small.

EISCAT_3D project
Most of the needed infrastructure for EISCAT_3D Stage 1 (E3DS1) was completed by the end of year. There are still few minor installations pending but the focus for 2024 is to install the radar electronics and later add the computer cluster needed for full scale data processing. Since Council decided to change the legal structure of the Association in the near future, it was also agreed that the process will be simpler if EISCAT_3D is kept as construction project until formally transferred into the EISCAT company.

The work of the Council and its committees
The EISCAT Council had two regular meetings and an extraordinary one in 2023. The first meeting in the year was a follow-on to the UK/hybrid autumn 2022 meeting. The regular spring meeting was a hybrid meeting with most members present in Skibotn and Tromsø, Norway. The regular autumn meeting was also held as hybrid with some members present in Qingdao, P. R. of China.

In the extraordinary meeting, the EISCAT Council committed *to transfer all of the Association's assets, operations, and commitments to a Swedish limited liability company to be owned by the three host countries, Finland, Norway, and Sweden.* The transfer is expected to happen in 2024. Sweden is taking the lead on detailing all necessary steps, legalities, etc.

The regular Council meetings during the year handled usual matters but also served as a forum for continued discussions about the future EISCAT company. The Council committees, the Administrative and Finance Committee (AFC) and the Scientific Advisory Committee (SAC) both had two hybrid meetings each during the year.

Budget development during the year
The 2023 operations ended below the budgeted target. One reason for the reduced operations was the problem with an antenna-gearbox on Svalbard which meant that experiments using different pointing directions could not be performed. A new gearbox was

ordered and has now arrived on Svalbard. Less operations meant reduced costs but funding from the Associates and Affiliates became less than planned. Reason being that one Associate had planned a funding increase for 2023, provided EISCAT_3D would be operational. Since that did not happen, the increase was not possible. This had also an effect on the EISCAT_3D finances, which needed to be adjusted to handle the reduced funding. In summary, the year ended in a balanced result.

The long-term budget plan
Since it is assumed that 2024 will be the last year for EISCAT Scientific Association, no long-term planning has been done. The budgeting and long-term planning for the EISCAT company will be handled by the new board and management.

The result for 2023 and profit/loss handling
The year ended in a balanced result.

PROFIT AND LOSS ACCOUNTS

in thousands of Swedish Crowns

	Note 1	*2023*	*2022*
Income from operations			
Grants received	Note 2	139 726	157 694
Revenue from operations	Note 3	0	0
Other income from operations	Note 4	164	83
		139 890	157 778
Expenses from operations			
Operation costs	Note 5	-8 500	-17 541
Administration costs		-3 265	-3 002
Personnel costs	Note 6	-28 357	-29 581
Depreciation of fixed assets		-7 439	-8 720
		-47 562	-58 843
Operating profit/loss		**92 328**	**98 935**
Financial items			
Interest income		3 530	1 442
Other financial income and cost		168	-1 695
		3 699	-253
Other items			
Income from sold inventory		11	37
Net profit/loss for the year		**96 037**	**98 718**

Changes in designated funds	Note 7		
Net profit/loss for the year		96 037	98 718
Use of designated investment funds		-70 583	-75 099
Use of other designated funds		-247	-1 002
Allocation of unused designated investment and other funds		-25 207	-22 116
Net profit/loss for the year after redistributions		**0**	**501**

BALANCE SHEET

in thousands of Swedish Crowns

		2023	*2022*
ASSETS			
Fixed assets			
Tangible fixed assets	Note 8		
Buildings		104 357	84 976
Radar systems		317 907	268 551
Equipment and tools		4 374	2 538
		426 638	356 065
Current assets			
Receivables		10 248	4 394
Prepayments and accrued income	Note 9	2 555	4 434
Cash at bank and in hand	Note 10	139 166	232 988
		151 969	241 816
Total assets		**578 607**	**597 881**
CAPITAL AND LIABILITIES			
Capital			
Funds invested	Note 11	426 638	356 065
Designated funds	Note 12	81 559	76 452
Net income for the year after redistribution		0	501
		508 197	433 018
Current liabilities			
Accounts payable, trade		7 400	33 682
EISCAT_3D build grants received but not used	Note 13	59 345	125 395
External project grants received but not used	Note 14	1 743	4 416
Other liabilities		1 921	1 371
		70 410	164 863
Total capital and liabilities		**578 607**	**597 881**

STATEMENT OF CASH FLOWS

in thousands of Swedish Crowns

	2023	*2022*
Operating activities		
Operating result before financial items	92 328	98 935
Depreciation of fixed assets	7 439	8 720
Interest received	3 530	1 442
Financial income and cost	168	-1 695
Other income and cost	11	37
Increase/decrease of receivables	-5 854	-2 425
Increase/decrease of prepayments and accrued income	1 879	-1 425
Increase/decrease of creditors and liabilities	-94 453	-99 028
Adjustment for items not included in cash flow	-20 848	-16 067
Cash flow from operations	**-15 800**	**-11 507**
Investment activities		
Investments in tangible assets	-78 022	-83 819
Cash flow from investment activities	**-78 022**	**-83 819**
Cash flow for the year	**-93 822**	**-95 326**
Liquid assets at the beginning of the year	**232 988**	**328 314**
Liquid assets at the end of the year	**139 166**	**232 988**

NOTES	2023	2022

Note 1 *Accounting principles*

The accounting and valuation principles applied are consistent with the provisions of the Swedish Annual Accounts Act and generally accepted accounting principles (for 2017 onwards, bokföringsnämnden allmänna råd och vägledningar, BFNAR 2012:1 K3).

All amounts are in thousands of Swedish kronor (SEK) unless otherwise stated.

Income
Received grants are reported as income in the period when they were claimed or received. Conditional grants are recognised as income when the associated conditions have been met. Income and revenue from operations, which include own-account funds, are reported as income when they were claimed or received. Grants and other income in foreign currencies have been accounted in the amounts estimated to be received, based on individual assessment.

Employee benefits
Ongoing remuneration to employees, either direct employed or provided via host agreements, in the form of salaries, social security, contributions to pension schemes and staff related insurances are accounted as personnel costs. Other remunerations, in cash, like travel subsistences or as benefits in-kind, like clothing, training and health care are also accounted as personnel costs. Overhead cost on host provided personnel is considered as external services accounted as administration cost.

Financial income
Dividends and interest income are accounted when credited the account.

Receivables
Receivables are stated at the amounts estimated to be received, based on individual assessment.

Receivables and payables in foreign currencies
Receivables and payables in foreign currencies are valued at the closing day rate. Where hedging measures have been used, such as forwarding contracts, the agreed exchange rate is applied. Gains and losses relating to operations are accounted for under other financial income and cost.

Bank accounts in foreign currencies
Bank balances in foreign currencies are valued at the closing day rate.

Fixed assets
Tangible fixed assets are stated at their original acquisition values after deduction of depreciation according to plan. Assets are depreciated systematically over their estimated useful lives. The following periods of depreciation are applied: Buildings 5 - 50 years, Radar systems 3 - 30 years and Equipment and tools 1 - 5 years.

Note 2 *Grants received*

The Associates contributed to the operation during the year in accordance with the EISCAT agreement and later additions. The Affiliates contributed according to agreed annual commitments. Income from European Commission (EC) funded projects were also accounted as received grants. The E3DS1 project started 2017-09-01 and the resulting projects costs were covered by the Associates (see Note 13) and other funds. Received project grants from the Associates are first accounted as prefinancing. Project costs are thereafter covered by withdrawals from prefinancing and at that time accounted as income from operations.

	2023	2022
Associates	40 814	40 874
Affiliates	1 403	1 585
Project grants, EC	2 804	3 853
Project grant, E3DS1	94 705	111 382
	139 726	157 694

Accumulated Associate contributions status as of 2023-12-31
Annual contributions included and for 2023, Finland, Japan (in-kind) and Norway were credited for providing E3DS1 project-related funds. These sums are used for EISCATs ownership and time-share calculation

Associate P. R. of China	62 162	57 710
Associate Finland	208 070	173 587
Associate Japan	129 104	126 684
Associate Norway	463 963	416 481
Associate Sweden	328 937	317 597
Associate UK	323 304	320 465
Previous Associates	382 168	382 168
	1 897 708	1 794 691

Note 3 *Revenue from operations*

The Association can, at rates related to the costs involved and as available, sell observation hours to Associates, Affiliates and other parties. Income from such selling of time are considered to be revenue. In 2023, no time-buyers used the systems.

Income from time-buyers	0	0

Note 4 *Other income from operations*

The Association supports visiting users by offering site accommodation and equipment hosting for either campaign brought instruments or for longer deployments. Educational support is done by providing teachers and/or other resources (like laboratory support).

Accommodation	107	33
Instrument hosting agreements	21	21
Educational support	23	23
Other income	14	7
	164	83

Note 5 *Operations*

The operating target for 2023 was 2 250 hours and the outcome became 1 952 hours. Passive hours come in addition. Such hours have a minimal effect on cost since the systems do not draw more electricity than in an off mode. Accounted hours are usually lower than the sum of operating hours since some systems have a charge rate that is less than 1-to-1.

Active hours (high-power), per system	*Hours*	*Hours*
EISCAT Svalbard Radar	685	637
UHF system	932	896
VHF system	288	384
Heating system	48	49
	1 952	1 966
Passive hours (receive only)		
UHF system	4	0
Kiruna receiver system	0	132
Sodankylä receiver system	0	132
	4	264

	2023	2022
Accounted hours	*Hours*	*Hours*
Common programmes	929	768
Special programmes	930	1 046
Other hours	98	194
	1 957	2 007
Distribution of special programme hours between Associates		
Associate P. R. of China	15	59
Associate Finland	145	153
Associate Japan	103	123
Associate Norway	267	254
Associate Sweden	181	208
Associate UK	173	153
All Associates, AA-runs	48	96
	930	1 046
Distribution, other hours		
Affiliates	58	140
EISCAT staff and tests	0	0
Peer-reviewed and TNA campaigns	40	54
Timebuyers	0	0
	98	194

Note 6 *Personnel costs and average number of employees*

The Association employs directly Headquarters and most project staff, currently about 18 positions, including the Director. The Headquarters is located in Kiruna, Sweden. The personnel working at the Kiruna (Sweden), Sodankylä (Finland), Svalbard and Tromsø (Norway) sites are normally not employed by the Association. Instead, the personnel are provided via site contracts by the Swedish Institute of Space Physics (Kiruna site staff but currently none), Oulu University (Sodankylä staff) and the Arctic University of Norway (Tromsø and Svalbard staff). The Association refunds all expenses related to the provided staff, as well as an additional overhead.

Personnel costs in total		
Salaries and emoluments paid to the Director	1 647	2 418
Other personnel, employed and provided via site contracts	17 466	17 553
Social security contributions amounted to	8 676	9 064
of which for pension costs	*4 068*	*4 318*
Other personnel costs	568	546

The current Director is Dr. Axel Steuwer. He assumed the role as Director 2023-01-01. His employment is for initially five years.

Of the pension costs, 294 kSEK (373 kSEK) relates to the Director. The Director and all other directly employed staff are included in individual occupational pension plans. For the personnel provided via site contracts, the pension plans are handled by their respective employer.

The members of the board (EISCAT Council) and members of committees, who represents Associates and Affiliates, do not receive remunerations from the Association. Travel expenses in connection with Council and committee meetings are normally covered by the Associates and Affiliates. The Association reimburses though the travel costs for Committee Chairpersons and external members.

	2023	2022
Salaries and emoluments and average number of staff per country		
Finland		
Salaries and emoluments	620	718
Average number of staff - men and women	1 + 0	1 + 0
Norway (including Svalbard)		
Salaries and emoluments	4 425	4 612
Average number of staff - men and women	6 + 0	7 + 0
Sweden		
Salaries and emoluments	14 067	14 641
Average number of staff - men and women	14 + 4	15 + 4

Members of the board and Directors at year-end - men and women

The board consist of delegations from every Associate country each having a Delegate (formal member) and up to two Representatives.

Board members (EISCAT Council)	10 + 4	11 + 3
Directors	1 + 0	1 + 0

Note 7 *Changes in designated funds*

Positive numbers - use of designated funds. Negative - transfer to the designated reserves or funds for later use.

Net profit/loss for the year	96 037	98 718
Transfers between regular EISCAT and EISCAT_3D construction project	-20 848	-16 067
Changes to capital operating reserve	-231	-100
Changes to decommissioning fund	-2 484	-2 651
Changes to E3D construction reserve	-3 182	-3 397
Changes to five-year operating reserve	1 306	0
Changes to funds invested	-70 583	-75 099
Changes to spare parts reserve	-16	-15
Changes to surplus fund	0	-887
	0	501

Note 8 *Tangible fixed assets*

Changes in tangible fixed assets.

Buildings		
Opening acquisition value	127 135	115 783
Acquisitions during the year	19 885	11 353
Disposals during the year	-10	0
Closing acquisition value	147 010	127 135
Opening accumulated depreciation	-42 160	-41 668
Depreciations during the year	-494	-491
Disposals during the year	0	0
Closing accumulated depreciation	-42 653	-42 160
Closing residual value	104 357	84 976
Radar systems		
Opening acquisition value	547 611	476 572
Acquisitions during the year	55 269	71 039
Disposals during the year	0	0
Closing acquisition value	602 880	547 611
Opening accumulated depreciation	-279 061	-271 830
Depreciations during the year	-5 913	-7 231
Disposals during the year	0	0
Closing accumulated depreciation	-284 974	-279 061
Closing residual value	317 907	268 551

	2023	2022
Equipment and tools		
Opening acquisition value	37 424	36 557
Acquisitions during the year	2 868	1 427
Disposals during the year	-7	-559
Closing acquisition value	40 285	37 424
Opening accumulated depreciation	-34 886	-34 448
Depreciations during the year	-1 032	-997
Disposals during the year	7	559
Closing accumulated depreciation	-35 911	-34 886
Closing residual value	4 374	2 538
Sum tangible fixed assets	426 638	356 065

Note 9 *Prepayments and accrued income*

Resources in staff and direct costs spent in ongoing externally funded projects are covered by accrued income until settled by submission of periodic report claims. In 2023, both EGI-ACE and ENVRI-FAIR had final report claims.

Prepaid rents	4	9
Prepaid insurances	355	1 107
Accrued income, EGI-ACE project	0	245
Accrued income, ENVRI-FAIR project	0	1 488
Accrued income, PITHIA-NRF project	1 673	342
Accrued income, other projects	128	24
Other items	394	1 220
	2 555	4 434

Note 10 *Bank balances status*

Nordea	139 166	232 988
Cash in hand	0	0
	139 166	232 988

Note 11 *Funds invested status*

Buildings	104 357	84 976
Radar Systems	317 907	268 551
Equipment and Tools	4 374	2 538
	426 638	356 065

Note 12 *Designated funds*

The designated funds are divided into funds and reserves. The Surplus fund and Five-year operating reserve are used for budget transfers between periods in the five years plan. The other funds are earmarked for specific purposes. The 2022 net profit was added to the surplus fund.

Capital operating reserve	3 485	3 254
E3D construction reserve	18 365	15 183
Decommissioning fund	14 333	11 850
Equipment repair fund	754	754
Five-year operating reserve	14 194	15 500
Investment fund	7 753	7 753
Restructuring reserve	4 101	4 101
Spare parts reserve	111	95
Surplus fund	18 463	17 962
	81 559	76 452

Note 13 *EISCAT_3D build grants received but not used*

The construction project, E3DS1, started 2017-09-01 and the completion of the first phase, Stage 1, is delayed. Most of the construction works were completed in 2023, but some remain and radar electronics will only be installed in 2024.

	2023	2022

Most Associates have committed to its realisation. An E3DS1 specific funding payment was received from Japan in 2023 and a transfer from the regular budget to the construction project was done, though less than planned. Associate funds are kept as prefinancing until used in the project. Funds spent are deducted from the different funding sources in accordance with the agreed funding plan.

Changes in EISCAT_3D build grants received but not used

Associate Finland		
Opening balance	43 009	62 567
Received during the year	0	0
Used during the year	-16 981	-19 557
Closing balance	26 028	43 009
Associate Japan		
Opening balance	10 214	16 367
Received during the year	2 585	1 108
Used during the year	0	-7 261
Closing balance	12 799	10 214
Associate Norway		
Opening balance	36 753	110 432
Received during the year	0	0
Used during the year	-35 629	-73 679
Closing balance	1 124	36 753
Associate Sweden		
Opening balance	0	10 884
Received during the year	0	0
Used during the year	0	-10 884
Closing balance	0	0
Regular EISCAT		
Opening balance	16 263	0
Received during the year	18 072	16 263
Used during the year	-33 155	0
Closing balance	1 179	16 263
E3DS1 project finances, gains/losses		
Opening balance	9 364	9 560
Changes during the year	2 776	-196
Closing balance	12 141	9 364
Local taxes Sweden contribution		
Opening balance	9 792	22 073
Received during the year	0	0
Used during the year	-3 718	-12 281
Closing balance	6 074	9 792
Sum EISCAT_3D received build grants	59 345	125 395

Note 14 *External project grants received but not used*

Most externally funded projects work with prefinancing. For European Commission projects, these are in EUR's. The prefinancing is used to cover reported and approved costs. The EGI-ACE and ENVRI-FAIR projects will be financially closed in 2024.

EGI-ACE H2020 prefinancing	-249	-42
ENVRI-FAIR H2020 prefinancing	-1 294	1 169
PITHIA-NRF H2020 prefinancing	3 285	3 289
	1 743	4 416

Appendix:

EISCAT Scientific Association Annual Report, 2024

EISCAT Scientific Association
Registered as a Swedish non-profit organisation
Organisation number: 897300-2549

Annual financial report for the year 2024-01-01 – 2024-12-31

The EISCAT Scientific Association submits herewith the annual report for 2024.

Content	Page
Administration report	2
Profit and loss accounts	4
Balance sheet	5
Statement of cash flows	6
Notes	7

ADMINISTRATION REPORT

Ownership, organisation and objective
The EISCAT Scientific Association was established in 1975 through an agreement between six European organisations. Japan joined in 1996 and the People's Republic of China in 2007.

The EISCAT Associates at 2024-12-31 are: China Research Institute of Radiowave Propagation (People's Republic of China), National Institute of Polar Research (Japan), Norges forskningsråd (Norway), Suomen Akatemia (Finland), UK Research and Innovation (United Kingdom of Great Britain and Northern Ireland) and Vetenskapsrådet (Sweden).

The now-running EISCAT Agreement came into force 2017-06-20, with all Associates making long term funding commitments to the Association. The Association has its formal seat in Kiruna, Sweden, and is registered as a non-profit organisation.

The aim of the Association is to make significant progress in the understanding of physical processes in geospace, in the high latitude atmosphere, and in the coupling between the high and low latitudes and altitudes. For this purpose, the Association has developed, constructed, and now operates, a number of radar facilities at high latitudes. At present, these comprise a system of stations at Tromsø (Norway), Kiruna (Sweden), Sodankylä (Finland), and Longyearbyen (Svalbard). The new system, EISCAT_3D, is currently being constructed.

The Association is fully funded by the Associates, but additional operations may also be funded by short term additional contributions from both Associate and non-Associate bodies. Depending on the available funding, scientific priorities and operational targets are adjusted on an annual basis.

Operation and scientific development
The EISCAT radar systems operated 1 862 hours in 2024 (1 957 hours in 2023).

Common Programmes amounted to 41% (47.5%) of the operations. Special Programmes amounted to 48% (47.5%) and other operations amounted to 11% (5%) of the total hours.

Affiliates from Germany, Portugal, South Korea, United Kingdom and USA made use of their access to the systems and totally 112 hours (58 hours) were accounted the affiliates. The Peer-Review Programme (PP) made it possible for user groups from Japan, United Kingdom and USA to run experiments, at no cost, on the systems. PP-time amounted to 76 accounted hours (40 hours). Transnational Access (TNA) project, PITHIA-NRF, funded campaigns in 2024 totalled 21 hours (0 hours).

Future operations and developments
With the already agreed change to a new organisational structure, EISCAT AB, 2024 was the last year of EISCAT Scientific Association operations. From 2025, all assets, developments, and operations are the responsibility of the new company.

The work of the Council and its committees

On 27 November 2024, the EISCAT Council Chairperson of the Association signed the Asset Transfer Agreement between EISCAT Scientific Association and EISCAT AB stating that *EISCAT Scientific Association undertakes to transfer to EISCAT AB at Closing, all rights, title, and interest in and to the EISCAT Association's property and assets, both tangible and intangible, that are owned, leased, held, or used (or intended for use) by the EISCAT Scientific Association on the Closing Date and that, directly or indirectly, relate to EISCAT (collectively, the "Acquired Assets"). EISCAT AB undertakes to assume from the EISCAT Association at Closing all such rights, title, and interest in or to the Acquired Assets.*

The Closing Date was set to *take place at the close of business on 2024-12-31. For the avoidance of doubt, the day on which EISCAT AB shall take possession shall be 2025-01-01.*

Regarding activities in 2024: The EISCAT Council had two regular meetings and an extraordinary one in 2024. The regular spring meeting was held in June 2024 as an in-person meeting in Tokyo, Japan. An extraordinary meeting then followed in September 2024 and a final in-person meeting was held at Vetenskapsrådet, in Stockholm, Sweden, November 2024. The November meeting was the final ordinary Council meeting of the Association. The needed final closure meeting of EISCAT Scientific Association will be held as a letter exchange session in spring 2025. The Council committees, the Administrative and Finance Committee (AFC) and the Scientific Advisory Committee (SAC) had also meetings during the year.

Budget development during the year

The 2024 operations ended below the budgeted target. Both the mainland radars and the EISCAT Svalbard Radar suffered from technical issues resulting in less operations than planned. The planned operating hours target was 2 618 hours, but the systems ran only 1 862 hours. The technical issues are mostly solved now. Less operations allowed staff to spend time on system improvements and more preventive maintenance works, including system tuning. In summary the year ended in a balanced result.

The long-term budget plan

Since 2024 was the last year for EISCAT Scientific Association, no long-term planning has been done. The budgeting and long-term planning for EISCAT AB is now handled by the company board and management.

The result for 2024 and profit/loss handling

The year ended in a balanced result.

PROFIT AND LOSS ACCOUNTS

in thousands of Swedish Crowns

	Note 1	*2024*	*2023*
Income from operations			
Grants received	Note 2	65 138	139 726
Revenue from operations	Note 3	0	0
Other income from operations	Note 4	126	164
		65 264	139 890
Expenses from operations			
Operation costs	Note 5	-10 896	-8 500
Administration costs		-3 068	-3 265
Personnel costs	Note 6	-29 398	-28 357
Depreciation of fixed assets		-6 729	-7 439
		-50 090	-47 562
Operating profit/loss		**15 173**	**92 328**
Financial items			
Interest income		3 255	3 530
Other financial income and cost		4 787	168
		8 042	3 699
Other items			
Income from sold inventory		242	11
Net profit/loss for the year		**23 457**	**96 037**

Changes in designated funds	Note 7	
Net profit/loss for the year	23 457	96 037
Use of designated investment funds	-2 551	-70 583
Use of other designated funds	-2 858	-247
Allocation of unused designated investment and other funds	-18 049	-25 207
Net profit/loss for the year after redistributions	**0**	**-0**

BALANCE SHEET

in thousands of Swedish Crowns

		2024	2023
ASSETS			
Fixed assets			
Tangible fixed assets	Note 8		
Buildings		111 141	104 357
Radar systems		313 462	317 907
Equipment and tools		4 581	4 374
		429 184	426 638
Current assets			
Receivables		3 781	10 248
Prepayments and accrued income	Note 9	1 573	2 555
Cash at bank and in hand	Note 10	197 559	139 166
		202 913	151 969
Total assets		**632 097**	**578 607**
CAPITAL AND LIABILITIES			
Capital			
Funds invested	Note 11	429 184	426 638
Designated funds	Note 12	80 332	81 559
Net income for the year after redistribution		0	0
		509 516	508 197
Current liabilities			
Accounts payable, trade		10 736	7 400
EISCAT_3D build grants received but not used	Note 13	104 702	59 345
External project grants received but not used	Note 14	3 984	1 743
Other liabilities		3 159	1 921
		122 581	70 410
Total capital and liabilities		**632 097**	**578 607**

STATEMENT OF CASH FLOWS

in thousands of Swedish Crowns

	2024	*2023*
Operating activities		
Operating result before financial items	15 173	92 328
Depreciation of fixed assets	6 729	7 439
Interest received	3 255	3 530
Financial income and cost	4 787	168
Other income and cost	242	11
Increase/decrease of receivables	6 467	-5 854
Increase/decrease of prepayments and accrued income	982	1 879
Increase/decrease of creditors and liabilities	52 171	-94 453
Adjustment for items not included in cash flow	-22 134	-20 848
Cash flow from operations	**67 672**	**-15 800**
Investment activities		
Investments in tangible assets	-9 279	-78 022
Cash flow from investment activities	**-9 279**	**-78 022**
Cash flow for the year	**58 393**	**-93 822**
Liquid assets at the beginning of the year	**139 166**	**232 988**
Liquid assets at the end of the year	**197 559**	**139 166**

NOTES	2024	2023

Note 1 *Accounting principles*

The accounting and valuation principles applied are consistent with the provisions of the Swedish Annual Accounts Act and generally accepted accounting principles (for 2017 onwards, bokföringsnämnden allmänna råd och vägledningar, BFNAR 2012:1 K3).

All amounts are in thousands of Swedish kronor (SEK) unless otherwise stated.

Income

Received grants are reported as income in the period when they were claimed or received. Conditional grants are recognised as income when the associated conditions have been met. Income and revenue from operations, which include own-account funds, are reported as income when they were claimed or received. Grants and other income in foreign currencies have been accounted in the amounts estimated to be received, based on individual assessment.

Employee benefits

Ongoing remuneration to employees, either direct employed or provided via host agreements, in the form of salaries, social security, contributions to pension schemes and staff related insurances are accounted as personnel costs. Other remunerations, in cash, like travel subsistences or as benefits in-kind, like clothing, training and health care are also accounted as personnel costs. Overhead cost on host provided personnel is considered as external services accounted as administration cost.

Financial income

Dividends and interest income are accounted when credited the account.

Receivables

Receivables are stated at the amounts estimated to be received, based on individual assessment.

Receivables and payables in foreign currencies

Receivables and payables in foreign currencies are valued at the closing day rate. Where hedging measures have been used, such as forwarding contracts, the agreed exchange rate is applied. Gains and losses relating to operations are accounted for under other financial income and cost.

Bank accounts in foreign currencies

Bank balances in foreign currencies are valued at the closing day rate.

Fixed assets

Tangible fixed assets are stated at their original acquisition values after deduction of depreciation according to plan. Assets are depreciated systematically over their estimated useful lives. The following periods of depreciation are applied: Buildings 5 - 50 years, Radar systems 3 - 30 years and Equipment and tools 1 - 5 years.

Note 2 *Grants received*

The Associates contributed to the operation during the year in accordance with the EISCAT agreement and later additions. The Affiliates contributed according to agreed annual commitments. Income from European Commission (EC) funded projects were also accounted as received grants. The E3DS1 project started 2017-09-01 and the resulting projects costs were covered by the Associates (see Note 13) and other funds. Received project grants from the Associates are first accounted as prefinancing. Project costs are thereafter covered by withdrawals from prefinancing and at that time accounted as income from operations.

	2024	2023
Associates	40 665	40 814
Affiliates	2 951	1 403
Project grants, EC	1 477	2 804
Project grant, E3DS1	20 044	94 705
	65 138	139 726

Accumulated Associate contributions status as of 2024-12-31

Annual contributions included and for 2024, Finland (cash and in-kind), Japan (in-kind), Norway and Sweden were credited for providing E3DS1 project-related funds. These sums are used for EISCATs ownership and time-share calculation. For 2024 a new accounting principle was retroactively introduced where the Associate contributions are credited in full when the funds are received rather than when used.

Associate P. R. of China	66 637	62 162
Associate Finland	275 234	208 070
Associate Japan	144 691	129 104
Associate Norway	489 459	463 963
Associate Sweden	378 610	328 937
Associate UK	326 211	323 304
Previous Associates	382 168	382 168
	2 063 011	1 897 708

Note 3 *Revenue from operations*

The Association can, at rates related to the costs involved and as available, sell observation hours to Associates, Affiliates and other parties. Income from such selling of time are considered to be revenue. In 2024, no time-buyers used the systems.

Income from time-buyers	0	0

Note 4 *Other income from operations*

The Association supports visiting users by offering site accommodation and equipment hosting for either campaign brought instruments or for longer deployments. Educational support is done by providing teachers and/or other resources (like laboratory support).

Accommodation	80	107
Instrument hosting agreements	21	21
Educational support	25	23
Other income	-0	14
	126	164

Note 5 *Operations*

The operating target for 2024 was 2 618 hours and the outcome became 1 862 hours. No passive (receive-only) hours in 2024.

Active hours (high-power), per system	*Hours*	*Hours*
EISCAT Svalbard Radar	528	685
UHF system	930	932
VHF system	347	288
Heating system	58	48
	1 862	1 952
Passive hours (receive only)		
UHF system	0	4
Kiruna receiver system	0	0
Sodankylä receiver system	0	0
	0	4

	2024	2023
Accounted hours	*Hours*	*Hours*
Common programmes	756	929
Special programmes	896	930
Other hours	210	98
	1 861	1 957
Distribution of special programme hours between Associates		
Associate P. R. of China	15	15
Associate Finland	104	145
Associate Japan	78	103
Associate Norway	223	267
Associate Sweden	225	181
Associate UK	170	173
All Associates, AA-runs	82	48
	896	930
Distribution, other hours		
Affiliates	112	58
EISCAT staff and tests	1	0
Peer-reviewed and TNA campaigns	97	40
Time-buyers	0	0
	210	98

Note 6 *Personnel costs and average number of employees*

The Association employs directly Headquarters and most project staff, currently about 17 positions, including the Director. The Headquarters is located in Kiruna, Sweden. The personnel working at the EISCAT sites are normally not employed by the Association. Instead, the personnel are provided via site contracts by the Swedish Institute of Space Physics (Kiruna site staff but currently none), Oulu University (Sodankylä staff but in 2024, no regular staff) and the Arctic University of Norway (Tromsø and Svalbard staff). The Association refunds all expenses related to the provided staff, as well as an additional overhead.

Personnel costs in total		
Salaries and emoluments paid to the Director	1 559	1 647
Other personnel, employed and provided via site contracts	18 932	17 466
Social security contributions amounted to	8 402	8 676
of which for pension costs	*3 753*	*4 068*
Other personnel costs	504	568

The current Director is Dr. Axel Steuwer. He assumed the role as Director 2023-01-01. With the changes to the organisational structure, his position as Director ended 2024-12-31. His employment will end few months into 2025.

Of the pension costs, 496 kSEK (294 kSEK) relates to the Director. The Director and all other directly employed staff are included in individual occupational pension plans. For the personnel provided via site contracts, the pension plans are handled by their respective employer.

The 249 kSEK 2024 staff cost in Finland relates to 2023.

The members of the board (EISCAT Council) and members of committees, who represents Associates and Affiliates, do not receive remunerations from the Association. Travel expenses in connection with Council and committee meetings are normally covered by the Associates and Affiliates. The Association reimburses though the travel costs for Committee Chairpersons and external members.

	2024	2023
Salaries and emoluments and average number of staff per country		
Finland		
Salaries and emoluments	249	620
Average number of staff - men and women	0 + 0	1 + 0
Norway (including Svalbard)		
Salaries and emoluments	5 872	4 425
Average number of staff - men and women	7 + 0	6 + 0
Sweden		
Salaries and emoluments	14 369	14 067
Average number of staff - men and women	12 + 5	14 + 4

Members of the board and Directors at year-end - men and women

The board consist of delegations from every Associate country each having a Delegate (formal member) and up to two Representatives.

Board members (EISCAT Council)	11 + 4	10 + 4
Directors	1 + 0	1 + 0

Note 7 *Changes in designated funds*

Positive numbers - use of designated funds. Negative - transfer to the designated reserves or funds for later use.

Net profit/loss for the year	23 457	96 037
Transfers between regular EISCAT and EISCAT_3D construction project	-22 134	-20 848
Changes to capital operating reserve	-190	-231
Changes to decommissioning fund	-273	-2 484
Changes to E3D construction reserve	-350	-3 182
Changes to five-year operating reserve	4 707	1 306
Changes to funds invested	-2 551	-70 583
Changes to spare parts reserve	-15	-16
Changes to surplus fund	-2 652	0
	0	0

Note 8 *Tangible fixed assets*

Changes in tangible fixed assets.

Buildings		
Opening acquisition value	147 010	127 135
Acquisitions during the year	7 278	19 885
Disposals during the year	0	-10
Closing acquisition value	154 289	147 010
Opening accumulated depreciation	-42 653	-42 160
Depreciations during the year	-494	-494
Disposals during the year	0	0
Closing accumulated depreciation	-43 148	-42 653
Closing residual value	111 141	104 357
Radar systems		
Opening acquisition value	602 880	547 611
Acquisitions during the year	272	55 269
Disposals during the year	0	0
Closing acquisition value	603 153	602 880
Opening accumulated depreciation	-284 974	-279 061
Depreciations during the year	-4 717	-5 913
Disposals during the year	0	0
Closing accumulated depreciation	-289 691	-284 974
Closing residual value	313 462	317 907

	2024	2023
Equipment and tools		
Opening acquisition value	40 285	37 424
Acquisitions during the year	1 729	2 868
Disposals during the year	-913	-7
Closing acquisition value	41 101	40 285
Opening accumulated depreciation	-35 911	-34 886
Depreciations during the year	-1 517	-1 032
Disposals during the year	908	7
Closing accumulated depreciation	-36 519	-35 911
Closing residual value	4 581	4 374
Sum tangible fixed assets	429 184	426 638

Note 9 *Prepayments and accrued income*

Resources in staff and direct costs spent in ongoing externally funded projects are covered by accrued income until settled by submission of periodic report claims.

Prepaid rents	9	4
Prepaid insurances	171	355
Accrued income, PITHIA-NRF project	1 239	1 673
Accrued income, other projects	0	128
Other items	153	394
	1 573	2 555

Note 10 *Bank balances status*

Nordea	197 559	139 166
Cash in hand	0	0
	197 559	139 166

Note 11 *Funds invested status*

Buildings	111 141	104 357
Radar Systems	313 462	317 907
Equipment and Tools	4 581	4 374
	429 184	426 638

Note 12 *Designated funds*

The designated funds are divided into funds and reserves. The Surplus fund and Five-year operating reserve are used for budget transfers between periods in the five years plan. The other funds are earmarked for specific purposes.

Capital operating reserve	3 675	3 485
E3D construction reserve	18 714	18 365
Decommissioning fund	14 606	14 333
Equipment repair fund	754	754
Five-year operating reserve	9 487	14 194
Investment fund	7 753	7 753
Restructuring reserve	4 101	4 101
Spare parts reserve	126	111
Surplus fund	21 115	18 463
	80 332	81 559

Note 13 *EISCAT_3D build grants received but not usea*

The construction project, E3DS1, started 2017-09-01 and the completion of the first phase, Stage 1, is delayed. Due to ground stability problems in Norway, and radar hardware issues, much of the planned final site installations works could not be done. Due to additional costs, Finland, Norway and Sweden agreed to supplement their earlier commitments.

	2024	2023
Changes in EISCAT_3D build grants received but not used		
Associate Finland		
Opening balance	26 028	43 009
Received during the year	17 796	0
Used during the year	-5 944	-16 981
Closing balance	37 880	26 028
Associate Japan		
Opening balance	12 799	10 214
Received during the year	704	2 585
Used during the year	0	0
Closing balance	13 503	12 799
Associate Norway		
Opening balance	1 124	36 753
Received during the year	12 435	0
Used during the year	-1 124	-35 629
Closing balance	12 435	1 124
Associate Sweden		
Opening balance	0	0
Received during the year	12 333	0
Used during the year	0	0
Closing balance	12 333	0
Regular EISCAT		
Opening balance	1 179	16 263
Received during the year	16 449	18 072
Used during the year	-12 976	-33 155
Closing balance	4 652	1 179
E3DS1 project finances, gains/losses		
Opening balance	12 141	9 364
Changes during the year	5 685	2 776
Closing balance	17 825	12 141
Local taxes Sweden contribution		
Opening balance	6 074	9 792
Received during the year	0	0
Used during the year	0	-3 718
Closing balance	6 074	6 074
Sum EISCAT_3D received build grants	104 702	59 345

Note 14 *External project grants received but not usea*

Most externally funded projects work with prefinancing. For European Commission projects, these are in EUR's. The prefinancing is used to cover reported and approved costs. The EGI-ACE and ENVRI-FAIR projects were financially closed in 2024. Two new EC-funded projects, ARC-TREE and INPROCAP started in 2024. A further project, RI-SCALE, was accepted by the Commission. It will start early 2025.

EGI-ACE H2020 prefinancing	0	-249
ENVRI-FAIR H2020 prefinancing	0	-1 294
PITHIA-NRF H2020 prefinancing	3 386	3 285
ARC-TREE H2023 prefinancing	170	0
INPROCAP H2023 prefinancing	428	0
RI-SCALE H2023 prefinancing (in 2025)	0	0
	3 984	1 743

Annual Report 2023–2024 of the EISCAT Scientific Association

EISCAT Headquarters
Box 812, SE-981 28 Kiruna, Sweden

Scientific contributions: EISCAT Associates and staff

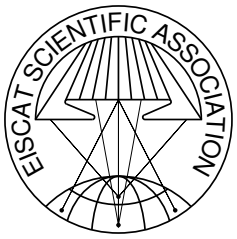

The EISCAT Associates

December 2024

CRIRP
China Research Institute of Radiowave Propagation
China
www.crirp.ac.cn

NFR
Forskningsrådet
Norway
www.forskningsradet.no

NIPR
National Institute of Polar Research
Japan
www.nipr.ac.jp

SA
Suomen Akatemia
Finland
www.aka.fi

UKRI
UK Research and Innovation
United Kingdom
www.ukri.org

VR
Vetenskapsrådet
Sweden
www.vr.se

EISCAT Scientific Association

Headquarters

EISCAT Scientific Association
Bengt Hultqvists väg 1
SE-981 92 Kiruna
Sweden
Phone: +46 980 79150
www.eiscat.se

Sites

Longyearbyen

EISCAT Svalbard Radar
Breinosa, Gruve7-veien
N-9171 Longyearbyen
Norway

Tromsø

EISCAT Tromsø Site
Ramfjordmoen
N-9027 Ramfjordbotn
Norway